



## Dive into Self-Supervised Learning for Medical Image Analysis: Data, Models and Tasks

arXiv:2209.12157v1 [cs.CV]

25 Sep 2022

Chuyan Zhang<sup>a</sup>, Yun Gu<sup>a</sup><sup>a</sup>*Institute of Medical Robotics, Shanghai Jiao Tong University, Shanghai, China*

### ARTICLE INFO

#### Article history:

2000 MSC: 41A05, 41A10, 65D05,  
65D17 Self-supervised Learning, Medical Imaging, Fine-tuning

### ABSTRACT

Self-supervised learning (SSL) has achieved remarkable performance on various medical imaging tasks by dint of priors from massive unlabeled data. However, for a specific downstream task, there is still a lack of an instruction book on how to select suitable pretext tasks and implementation details. In this work, we first review the latest applications of self-supervised methods in the field of medical imaging analysis. Then, we conduct extensive experiments to explore four significant issues in SSL for medical imaging, including (1) the effect of self-supervised pretraining on imbalanced datasets, (2) network architectures, (3) the applicability of upstream tasks to downstream tasks and (4) the stacking effect of SSL and commonly used policies for deep learning, including data resampling and augmentation. Based on the experimental results, potential guidelines are presented for self-supervised pretraining in medical imaging. Finally, we discuss future research directions and raise issues to be aware of when designing new SSL methods and paradigms.

© 2022 Elsevier B. V. All rights reserved.

### 1. Introduction

Transfer learning from external data has become the mainstream technology of deep learning to deal with the annotated data scarcity in medical imaging. The de facto standard pipeline consists of two steps: 1) a convolutional neural network (CNN) is first pretrained on a source dataset. 2) the pretrained network is then fine-tuned using limited annotated data with an adaptation layer added on the top of its architecture for a specific target task (Oquab et al., 2014). It is generally understood that the merits of transfer learning are contributed by the feature-reuse and low-level statistics from pretrained models (Neyshabur et al., 2020). Driven by the desire to reduce the manual annotations of source data, self-supervised learning (SSL) is progressively overtaking the fully-supervised learning (FSL) as the top of the table for the pretraining paradigms in state-of-the-art computer vision (Ericsson et al., 2021; Islam et al., 2021; Hosseinzadeh Taher et al., 2021).

SSL formulates pretext tasks to encourage learning semantically useful representations from the unlabeled data, which can boost the performance of downstream tasks with limited annotated data. The design of these pretext tasks should encourage the networks to capture the high-level semantics rather than trivial features (Chen et al., 2019; Chowdhury et al., 2021). With the impressive achievements of SSL in computer vision, there are growing appeals for developing SSL techniques tailored to medical data. Thus far, a variety of studies have demonstrated the effectiveness of SSL approaches across various medical image

recognition tasks, including classification (Sowrirajan *et al.*, 2021; Zhou *et al.*, 2021b; Taher *et al.*, 2022; Haghghi *et al.*, 2022), detection/localization (Tajbakhsh *et al.*, 2019; Chen *et al.*, 2019; Benčević *et al.*, 2022), and segmentation (Taleb *et al.*, 2020; Tao *et al.*, 2020a; Xie *et al.*, 2020; Zhou *et al.*, 2021b; Taher *et al.*, 2022; Haghghi *et al.*, 2022).

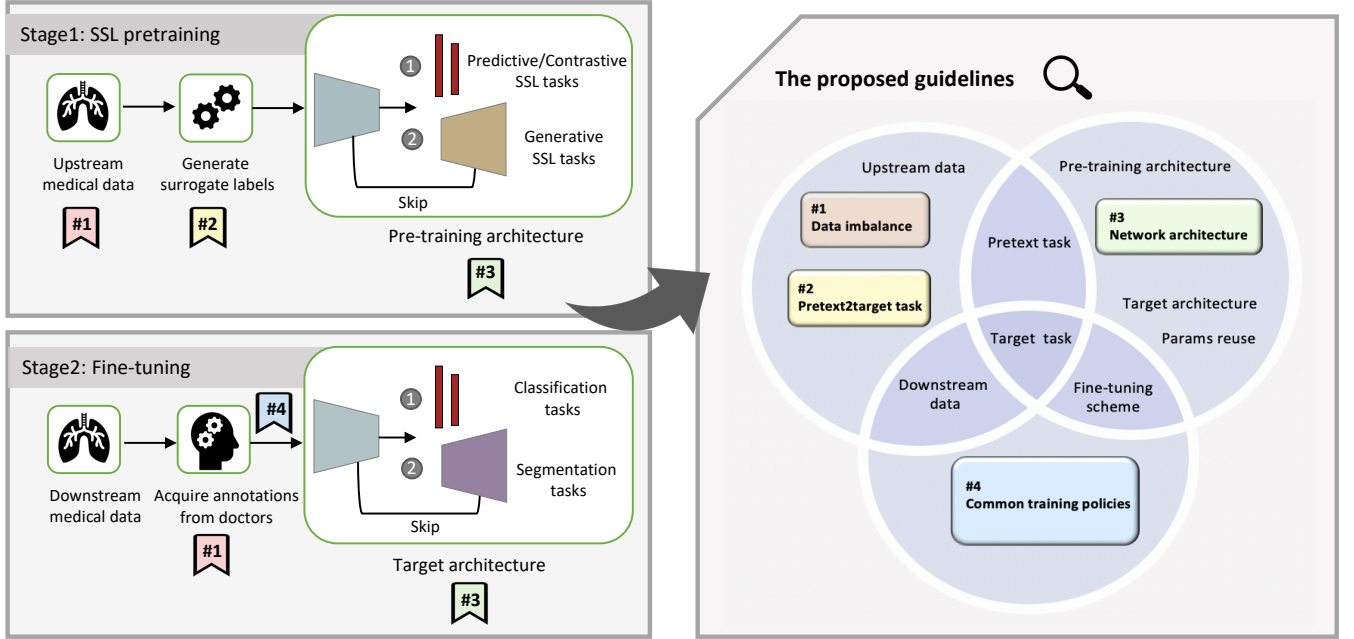


**Fig. 1.** The overview of the general paradigm of self-supervised learning in medical imaging. It includes two training stages, namely SSL pretraining and fine-tuning. Our proposed guidelines in four dimensions (1. Data imbalance; 2. network architecture; 3. Pretext tasks; 4. Common training policies) are remarked throughout the whole training process, involving data, models, tasks and transfer schemes.

In the medical context, SSL literatures mainly focus on creating novel pretext tasks and validating the improved performance of the self-supervised learned features. Recently, several systematic reviews of SSL literature have been undertaken (Xu, 2021; Chowdhury *et al.*, 2021; Shurab and Duwairi, 2022; Chen *et al.*, 2022). In addition to the performance evaluation, a few works discovered broader implications of SSL approaches, such as better robustness and generalization (Navarro *et al.*, 2021; Srinivasan *et al.*, 2021). Despite these preliminary attempts, there are still underexplored problems in the practice of “pretrain-then-finetune” paradigm. Firstly, given diverse pretext tasks with substantially different (formulations) core ideas, e.g. generative learning and contrastive learning (Liu *et al.*, 2021), which type of methods is empirically effective? This is hard to assess from current literature with potential experimental flaws, including incomplete comparison of limited types of SSL methods, inconsistent validity reported by the same method in different evaluation conditions and the biased selection of baselines. Secondly, data bias is a prominent issue in medical images since malignant samples are in the minority. In regular CNN training, data resampling and augmentations are widely adopted to improve class-imbalanced learning from the perspective of expanding the frequency of rare class. However, little attention has been paid to the behaviors of SSL algorithms under data imbalance. Furthermore, to get a clear picture of the utilities that SSL can provide, there is a necessity to investigate the additive effect of SSL with resampling or data augmentations. Thirdly, the success of SSL-based transfer learning depends on two imperative implementations: how to design a proper pretext task, and how to transfer useful representations from the pretrained model to downstream tasks? For the former question, inappropriate implementations of the pretext task might cause that the network finds trivial solutions as a shortcut to accomplish its goals. For the latter question, it is important to determine whether the self-supervised learned features are preserved active in downstream learning or not.

In this paper, we precisely fill this research gap by taking a closer look at the aforementioned problems. We first revisit prominent SSL techniques covering all the types and introduce an evaluation benchmark across three popular medical datasets for the underexplored issues in existing literature. Based on extensive experiments (nearly 250 experiments, 2000 GPU hours), we perform a fine-grained study and propose a series of guidelines for the community to exploit the capacity of SSL. Fig. 1 navigates the positions of our proposals during pretraining and fine-tuning, which can actually serve as a guidebook. As a result of this study, we uncover several crucial insights. The most significant observations are summarized as follows:

- SSL facilitates class-imbalanced problems with remarkable improvement on the minority class but marginal gains or occasional losses on the majority class.
- The data bias in pretraining data also affects the representation learning in SSL paradigm, leading to poor performance under extreme data imbalance. Data resampling can neutralize such skewed representations and yields mutual benefits with SSL.
- For encoder-decoder architectures, the representations in the pretrained encoder are more meaningful than the decoder as the decoder might impose the risk of overfitting to inductive information for solving the pretext task itself.
- SSL pretraining only offers substantial gains in the absence of data augmentation. When using strong data augmentation, most of the SSL methods hurt the segmentation performance, which highlights the need to rethink the value of SSL pretraining in medical segmentation tasks.

## 2. Self-Supervision Literature Review

As remarkable success has been made through SSL in the field of computer vision, SSL works are increasingly proposed for medical imaging analysis to relieve the issue of scarce annotations. This review is organized in three parts: firstly, we present a formal concept of SSL involving relevant terms and review previous SSL approaches in terms of four categories during the years 2019 to 2022. Secondly, we summarize previous literature reviews. Thirdly, we also survey the analytical works for deeply understanding SSL. In the final part, we distinguish our work from recent relevant papers.

### 2.1. *Self-supervised approaches in medical image analysis*

**Formal concept of SSL.** The core idea of SSL is to learn useful representations from the inherent information in unlabeled images by solving a pretext task (also called auxiliary or proxy task). According to the purpose of a certain pretext task, surrogate supervisory signals are automatically generated from an unlabeled dataset, called source dataset or upstream dataset. Rather than the pretext task itself, the true interest of users is the downstream task, e.g. image classification, semantic segmentation or object detection. In the notion of transfer learning, SSL pretraining is adopted as an alternative scheme to improve the performance of downstream tasks. Specifically, the SSL pretrained model is then transferred to a specific downstream task and fine-tuned with a labelled dataset, called target dataset or downstream dataset. According to the patterns of pretext tasks, SSL methods can be categorized into predictive SSL, generative SSL, contrastive SSL and multi-SSL.

**Predictive SSL: making transformation predictions.** Predictive pretext tasks learn the contextual or structural semantics via predicting geometric transformations of images. In these methods, the prediction of transformation is formulated as a classification problem, which maps input images or volumes to a scalar or vector in semantic space. The common transformation prediction-based tasks in computer vision field consider the relative positions (Doersch *et al.*, 2015), the rotation angles (Komodakis and Gidaris, 2018) and the jigsaw puzzles (Noroozi and Favaro, 2016) etc. A majority of works proved the effectiveness of these

traditional pretext tasks in medical imaging: Tajbakhsh *et al.* (Tajbakhsh et al., 2019) demonstrated that utilizing rotation prediction as a pretraining scheme for medical images is more effective than transfer learning from natural images. Taleb *et al.* (Taleb et al., 2020) presented 3D versions of relative patch location, rotation prediction and jigsaw puzzles for 3D medical applications. Some other works developed novel predictive SSL tasks on medical scenarios: Bai *et al.* (Bai et al., 2019) proposed to predict anatomical positions for cardiac MR image segmentation. Blendowski *et al.* (Blendowski et al., 2019) presented a new SSL approach by predicting orthogonal patch offsets. Zhuang *et al.* (Zhuang et al., 2019) designed a novel proxy task named “Rubik’s cube recovery” of predicting the cube orders and rotations in the same framework. Zhu *et al.* (Zhu et al., 2020) further extended “Rubik’s cube recovery” by adding a new sub-task of identifying whether a cube is masked or not. Nguyen *et al.* (Nguyen et al., 2020) exploited the spatial information inherent in medical data in the proposed SSL framework by corrupting slices in a small range and training a model to predict whether the slice is corrupted or not as well as the slice index. Li *et al.* (Li et al., 2021) introduced two predictive pretext tasks into the multiple instance learning framework for COVID-19 diagnosis: the relative patch location and an additional task of absolute patch location.

**Generative SSL: recovering the corrupted or masked part of the input.** The underlying idea of the generative pretext tasks is to learn context-aware features by recovering the distorted or unobserved image crops. Unlike predictive and contrastive SSL, generative SSL demands not only an encoder to extract compressed representations from input pixels, but also a decoder to convert the latent representations back to pixels. As the objective of reconstruction is always the original data, different transformations of the raw data give rise to a variety of pretext tasks, such as inpainting (Pathak et al., 2016) and colorization (Zhang et al., 2016; Larsson et al., 2017). Inspired by the common tasks in computer vision, Tajbakhsh *et al.* (Tajbakhsh et al., 2019) applied colorization in a conditional generative adversarial network (GAN) (Larsson et al., 2017) and patch reconstruction in a Wasserstein GAN (Arjovsky et al., 2017) and conducted experiments on multiple medical imaging tasks. Chen *et al.* (Chen et al., 2019) claimed that existing pretext tasks such as local context restoration (Larsson et al., 2017) often yield only marginal improvements on medical image datasets. To better exploit the rich information in unlabeled images, they proposed a new SSL strategy for context restoration, in which small patches are randomly switched in an image. As an extension of previous context-restoration-based works, Zhou *et al.* (Zhou et al., 2021b) integrated four data transformations into a unified reconstruction model, namely “Model Genesis”. Motivated by Rubik’s cube pretext tasks (Zhuang et al., 2019; Zhu et al., 2020), Tao *et al.* (Tao et al., 2020a) developed a new SSL task based on a GAN. Different from (Zhuang et al., 2019; Zhu et al., 2020), individual change of a sub-cube is forbidden and the movement of sub-cubes is bound to its adjacent sub-cubes. Instead of using the transformations in Rubik’s Cube to form a classification problem, they proposed a generative task of recovering the original image from the disrupted version and an adversarial task of distinguishing whether the cubes are in the correct arrangement.

**Contrastive SSL: learning maximum agreement between the embeddings of two views of one sample.** Contrastive learning aims at maximizing the mutual information between positive image pairs and minimizing the representation similarity of negative image pairs if necessary. In general, the positive pairs are two augmented views of one instance while the negative pairs are from different instances. The network can therefore capture discriminative representations of instances that are worthwhile for pattern recognition. Recently, contrastive learning has become one of the most popular trends in SSL and shows outstanding performance in a wide range of computer vision tasks, leading to a proliferation of related studies (Chen et al., 2020a; He et al., 2020; Chen et al., 2020b; Grill et al., 2020; Chen and He, 2021). However, mainstream contrastive SSL algorithms designed for object-centric natural images could be problematic for medical images with distinctive characteristics from natural images: (1) There is always a diverse set of object-of-interests and much more clinically-related background information in a medical image. (2)

The consistent anatomical structures in medical images cause subtle instance-wise differences, especially for Magnetic Resonance Imaging (MRI) and Computed Tomography (CT) scans. Through the exploitation of the above properties, many efforts have been made to enable the expansion of advanced contrastive SSL methods in medical images, including improvements on augmentations, mining strategy of positive and negative pairs, contrastive loss functions, etc. These works can be further categorized into two groups according to the target tasks: global-attention contrastive SSL for classification problems and local-attention contrastive SSL for pixel-wise segmentation problems. For global-attention methods, Sowrirajan *et al.* (Sowrirajan et al., 2021) claimed that the original augmentations in MOCO (He et al., 2020) are inappropriate for gray-scale medical images. For instance, random crop and blurring might eliminate the lesions. Therefore, they proposed the MoCo-CXR to fit into chest X-Ray images by modifying augmentations in MoCo. As another extension work of MoCo, Sriram et al. (Sriram et al., 2021) performed SSL pretraining on non-COVID datasets to benefit the downstream COVID-19 prediction. Based on MoCo-CXR, Vu *et al.* (Vu et al., 2021) present an SSL method named MedAug based on MOCO of generating positive pairs from possibly different images of one patient according to the metadata. Similar work to MedAug was proposed by Azizi *et al.* (Azizi et al., 2021), where they utilized SimCLR as the benchmarking framework and introduced a Multi-Instance Contrastive Learning (MICLe) for constructing more informative positive pairs from multiple images of the underlying pathology from the same patient. For local-attention methods, Chaitanya *et al.* (Chaitanya et al., 2020) proposed two alternatives to the SimCLR (Chen et al., 2020a) for 3D medical image segmentation. They designed a novel contrasting strategy based on the structural similarity in volumetric medical images and a local contrastive loss. Xie *et al.* (Xie et al., 2020) presented a Prior-Guided Local (PGL) SSL approach to improve BYOL (Grill et al., 2020) by learning the local consistency of the same region.

**Multi-SSL: combining multiple SSL pretext tasks into one framework.** Due to the limitation that single pretext task could learn task-biased features, multi-SSL adopts different self-supervision signals for networks training to obtain robust representations. In this section, we only review the SSL work that combines pretext tasks of different types (predictive, generative, contrastive). Based on Model Genesis, Haghghi *et al.* (Haghghi et al., 2020) proposed a Semantic Genesis framework to learn semantically enriched representation by self-restoration, self-discovery and self-classification, simultaneously. In the self-discovery stage, representations learned by an auto-encoder are compared to discover images from semantically similar patients. Then, they assign an anatomical pattern label for patches with fixed positions in these images. The self-classification and self-recovery refer to the pattern classification task and the reconstruction task in Model Genesis, respectively. As another extension work of Model Genesis, Zhang *et al.* (Zhang et al., 2021) added a scale-aware proxy task of predicting the scale of input cubes into the Model Genesis framework to learn multi-level local representations. Zhou *et al.* (Zhou et al., 2021a) incorporated contrastive and generative SSL into a PCRL framework, where "preservational learning" is proposed for the generative SSL to preserve more information. Dong *et al.* (Dong et al., 2021) designed a self-supervised multi-task framework consisting of a contrastive sub-task and a generative sub-task to simultaneously learn instance discrimination and the underlying structure from sequential 2D medical data. In the embedding space, the contrastive proxy task aims to maximize the similarity of slices from the same patient volume while minimize the similarity of slices from different patient. Given a slice, the objective of the generative task is recovering its precedent and successor slices within several steps in the same volume. Taher *et al.* (Taher et al., 2022) argued that state-of-the-art contrastive SSL algorithms aim at learning global instance-discrimination of photographic images while medical image analysis requires more attention to local features. Inspired by PCRL, they added a reconstruction task into the contrastive learning framework, thereby enabling finer and more discriminative features. To benefit from collaborative learning, Haghghi *et al.* (Haghghi et al., 2022) further developed DiRA by integrating discriminative, restorative, and adversarial Learning.

## 2.2. Previous reviews of self-supervised learning

Encouraged by the significant breakthroughs of SSL, extensive works have applied SSL techniques in medical imaging analysis to overcome the challenge of lacking sufficient labeled medical data to train reliable networks. Thus far, a series of studies have reviewed existing SSL approaches for medical images (Xu, 2021; Chowdhury *et al.*, 2021; Shurrab and Duwairi, 2022; Chen *et al.*, 2022). Most of the reviews were organized into an analogical structure, which is composed of the introduction, survey and discussion part. The introduction part always includes the background of SSL and the selection criteria of published papers to be reviewed. In the survey part, related works are detailed in terms of several defined categories. In the end, latest research trends, potential issues and future directions will be fully discussed to offer fresh perspectives on community.

## 2.3. Analytical work for understanding self-supervised learning

Despite the success of SSL in improving the performance of downstream tasks, the reasons behind the benefits of SSL remain largely unexamined. To enhance our understanding of SSL, there is a growing body of literature analyzing its properties in different settings through carefully designed experiments. Navarro *et al.* (Navarro *et al.*, 2021) pointed out that self-supervision only yields marginal performance improvements compared with full-supervised learning and they thus turned to assess the robustness and generalizability of SSL algorithms in medical datasets. The evaluations on disturbed images finally revealed the advantages of SSL in acquiring robust representations. Srinivasan *et al.* (Srinivasan *et al.*, 2021) paid much attention to the broader implications of SSL in the context of diabetic retinopathy, involving the specificities of the self-supervised learned features, the interpretability of SSL pre-trained models and robustness to distortions. Liu *et al.* (Liu *et al.*, 2021) explored the behaviors of SSL in data-imbalanced scenarios and discovered that the robustness of self-supervised learned representations to class imbalance prevails over supervised learned representations.

## 2.4. Position of our work

Currently, a few excellent reviews have established a comprehensive body of knowledge to facilitate researchers' understanding of different SSL methods. Furthermore, some analysis approaches help researchers better grasp the capabilities of SSL. However, choosing a conducive pretext task and executing it appropriately on a target task remains a complex problem for researchers: the results of a particular downstream task reported in previous SSL works always cover a small portion of SSL methods. In this work, we briefly review the relevant literature but concentrate more on an analysis part. Different from previous analytical works towards investigating one predominant property of SSL with very limited methods (sometimes encompassing only a single type of SSL like the contrastive SSL), we aim to consider a set of possible issues in practice and present detailed references for researchers working with SSL.

## 3. Study Methodology

In this study, a brief outline is first presented to cover the significant topics throughout the process of SSL applications. Then, we illustrate the selection of SSL methods. Afterwards, the setting of experiments are described with relevant medical datasets and downstream tasks. Finally, we discuss the potential limitations in the current literature. By implementing a unified benchmark framework, a fair comparison of representative SSL algorithms is performed across multiple medical tasks.

**Table 1. The outline of our study.** We conduct a fine-grained study on various topics, regarding the impact of SSL in four aspects. For each topic, we display the target task/tasks, which is/are selected considering the feasibility and simplicity.

Instructions	Target task	
	Classification	Segmentation
<b>Data imbalance</b>	Degrees of imbalance	✓ <span style="float: right;">✗</span>
	Performance on different classes	✓ <span style="float: right;">✓</span>
<b>Pretext tasks</b>	Selection of pretext tasks	✓ <span style="float: right;">✓</span>
	Input data size	✓ <span style="float: right;">✓</span>
<b>Network architecture</b>	Feature visualization	✓ <span style="float: right;">✗</span>
	Encoder	✓ <span style="float: right;">✓</span>
	Decoder	✗ <span style="float: right;">✓</span>
	Skip connections	✓ <span style="float: right;">✓</span>
<b>Common training policies</b>	Normalization layers	✓ <span style="float: right;">✓</span>
	Fine-tuning strategy	✓ <span style="float: right;">✓</span>
	Additive effect with data resampling	✓ <span style="float: right;">✗</span>
	Additive effect with data augmentation	✗ <span style="float: right;">✓</span>

### 3.1. Study Outline

The study is conducted with the issues listed in Table 1, including four major stages involved in upstream and downstream training phase. Each stage is carefully examined and analyzed with selected SSL methods on multiple datasets. Due to the different mechanisms of classification tasks and segmentation tasks, we included appropriate medical tasks for exploring various factors. For instance, the degree of class-imbalance for classification tasks is easier to adjust than segmentation tasks. Thus for simplicity, we only perform the experiments in the classification task. Based on extensive experiments, we finally provide detailed guidelines for a deeper understanding and more effective use of SSL pretraining. **The implementation details are available in the supplementary material.**

### 3.2. Selected SSL Methodology

As claimed in (Taleb *et al.*, 2020) and (Zhou *et al.*, 2021b), SSL methods contribute to larger improvements on 3D volumetric data. Therefore, we prioritize 3D SSL tasks with ten baseline methods, adequately covering the state-of-the-art for medical applications and spanning all the types we defined before. In total, five of these ten methods are predictive SSL (ROT (Komodakis and Gidaris, 2018), RPL (Doersch *et al.*, 2015), Jigsaw (Taleb *et al.*, 2020), RKB (Zhuang *et al.*, 2019) and RKB+ (Zhu *et al.*, 2020)), three are generative SSL (AE (Schmidhuber, 2015), MG (Zhou *et al.*, 2021b), PCRL Zhou *et al.* (2021a)<sup>1</sup>) and two are contrastive SSL (SimCLR (Chen *et al.*, 2020a), BYOL (Grill *et al.*, 2020)). Each of these is formally presented below.

**Rotation Prediction (ROT)** First proposed by (Komodakis and Gidaris, 2018) for 2D images, this pretext task learns representative features by predicting rotation angles from rotated inputs. The underlying idea is that for estimating orientations, the network has to capture recurrent structures, which is meaningful for object recognition. To harness the full spatial context of 3D medical volumes, Taleb *et al.* (Taleb *et al.*, 2020) modified the original task to a 3D version and framed the task as a 10-way classification problem: the input images are randomly rotated by one of  $\{0^\circ, 90^\circ, 180^\circ, 270^\circ\}$  along an arbitrary axis of  $\{x, y, z\}$ , leading to 10

<sup>1</sup>PCRL is categorized into Multi-SSL above.

**Table 2. Statistics of CT datasets in existing SSL works. Here Cls. denotes classification, Seg. denotes segmentation and Loc. denotes localization. We rank the datasets according to the usage frequency in publications.**

Name	# of annotated scans	Object	Task	Publication
LiTS 2017 (Bilic <i>et al.</i> , 2019)	130	Liver	Seg.	(Zhou <i>et al.</i> , 2021b)
				(Haghghi <i>et al.</i> , 2020)
				(Zhou <i>et al.</i> , 2021a)
				(Xie <i>et al.</i> , 2020)
LUNA 2016 (Setio <i>et al.</i> , 2017)	888	Lung Nodule	Cls.	(Zhou <i>et al.</i> , 2021b)
				(Haghghi <i>et al.</i> , 2020)
				(Zhou <i>et al.</i> , 2021a)
				(Tajbakhsh <i>et al.</i> , 2019)
LIDC-IDRI (Armato III <i>et al.</i> , 2011)	1018	Lung Nodule	Seg.	(Zhou <i>et al.</i> , 2021b)
				(Haghghi <i>et al.</i> , 2020)
LIDC-IDRI (Armato III <i>et al.</i> , 2011)	355	Lung Lobe	Seg.	(Tajbakhsh <i>et al.</i> , 2019)
MSD-Pancreas (Antonelli <i>et al.</i> , 2022)	420	Pancreas	Seg.	(Taleb <i>et al.</i> , 2020)
Abdominal multi-organ (Tong <i>et al.</i> , 2015)	150	Abdominal Organs	Loc.	(Chen <i>et al.</i> , 2019)
NIH-Pancreas (Roth <i>et al.</i> , 2015)	82	Pancreas	Seg.	(Tao <i>et al.</i> , 2020a)
PE-CAD (Tajbakhsh <i>et al.</i> , 2015)	121	Pulmonary Emboli	Cls.	(Zhou <i>et al.</i> , 2021b)

possible rotation strategies. Assuming  $K$  as the class numbers, the  $K$ -dim one-hot rotation label as  $y^{rot}$  and network prediction as  $p^{rot}$ , the objective function of the network is a simple cross-entropy loss:

$$L_{ROT} = - \sum_{j=1}^K y_j^{rot} \log p_j^{rot} \quad (1)$$

**Relative Patch Location (RPL)** Originally proposed in (Doersch *et al.*, 2015), this pretext task seeks to learn semantic representations by predicting the spatial position relations of patches in one image. In the 3D counterpart presented by (Taleb *et al.*, 2020), the input volumetric data is first partitioned into  $N$  cubes  $x_i, i = 1 \dots N$  in the form of a grid and then the central cube is regarded as a reference patch  $x_c$  while a query patch  $x_q$  is randomly chosen from the remaining  $N - 1$  patches. Obviously, there are 26 spatial location relations between  $x_c$  and  $x_q$ . Therefore, this task can be considered as a 26-way classification problem. To prevent the models from learning trivial solutions by the shortcut across two neighboring patches, e.g. edge continuity, random jitter is necessary between adjacent 3D patches. Here, the class number  $K$  becomes the number of cubes in a 3D grid except for the central one. Let  $y^{rpl}$  and  $p^{rpl}$  refer to the one-hot label and the predicted probability vector, respectively. Similar to ROT, the loss function of RPL can be expressed as:

$$L_{RPL} = - \sum_{j=1}^K y_j^{rpl} \log p_j^{rpl} \quad (2)$$

**Jigsaw puzzle solving (Jigsaw)** Following the intuition behind RPL, Jigsaw puzzle solving was proposed as a more complex SSL task in (Noroozi and Favaro, 2016) for 2D images. Different with RPL, the input image for this task is first split into  $n \times n$  cubes in the form of a grid and then permuted in some order. The goal of this task is to predict the right arrangement of shuffled input cubes, just like playing a jigsaw puzzle. For a 3D image, there exist  $n \times n \times n$  cubes and  $n^3$ ! possible arrangements which is oversize for network predicting. Therefore, Taleb *et al.* (Taleb *et al.*, 2020) proposed a simplified scheme of selecting  $K$  possible

orders with the largest Hamming distance, thereby casting the task to a K-way classification problem. Formally, let  $y^{jig}$  and  $p^{jig}$  refer to the one-hot label and the predicted probability vector, respectively. The loss function of Jigsaw can be expressed as:

$$L_{Jigsaw} = - \sum_{j=1}^K y_j^{jig} \log p_j^{jig} \quad (3)$$

**Rubik’s Cube (RKB)** Inspired by the early work on Jigsaw puzzle solving (Noroozi and Favaro, 2016; Taleb *et al.*, 2020), Zhuang *et al.* (Zhuang *et al.*, 2019) developed a novel pretext task, i.e. Rubik’s cube recovery, to deeply exploit the rich anatomical information in 3D images. To learn both translational and rotational invariant representations, they performed the pretext task of cube rearrangement and cube rotation prediction in a jointly learning framework. For an input volume,  $n \times n \times n$  shuffled cubes are generated in the same way in Jigsaw. Then, each cube  $x_i, i = 1 \dots N$  is randomly rotated by 180° vertically and horizontally. Hence, the supervision signals are three labels: a  $K$ -dim one-hot label  $y_{order}$  for cube orders, a  $N$ -dim multi-hot label  $y_{hor}$  for vertical rotation with 1 on the positions of vertically rotated cubes and 0 vice versa, and a  $N$ -dim multi-hot label  $y_{ver}$  for horizontal rotation. Assuming  $p_{order}$  as the order prediction, the loss function for the cube ordering sub-task is just the same as Jigsaw:

$$L_{order} = - \sum_{j=1}^K y_j^{order} \log p_j^{order} \quad (4)$$

Each of the two cube rotation sub-tasks can be solved as a multi-label binary classification problem. Assuming  $p_{hor}$  and  $p_{ver}$  as the horizontal and vertical rotation prediction, the loss function can be written as:

$$L_{rot} = - \left( \sum_{i=1}^N (y_i^{hor} \log p_i^{hor} + y_i^{ver} \log p_i^{ver}) \right) \quad (5)$$

In total, the loss function comprises the above two terms of sub-tasks:

$$L_{RKB} = \alpha L_{order} + \beta L_{rot} \quad (6)$$

**Rubik’s Cube+ (RKB+)** Following the idea that a harder pretext task often enables more robust feature representations (Wei *et al.*, 2019), Zhu *et al.* (Zhu *et al.*, 2020) added a new sub-task of cube masking identification to RKB. After the transformations for cubes in RKB, each cube is then randomly masked with a possibility of 0.5 at each voxel. In addition to the two sub-tasks in the original RKB, the network is trained to identify whether each cube is masked or not, which can be cast as a multi-label binary classification problem. The ground truth for cube masking is a  $N$ -dim multi-hot label  $y_{mask}$  with 1 on the positions of masked cubes and 0 vice versa. Let  $p_{mask}$  denote network prediction for masking identification, its loss function can be expressed as:

$$L_{mask} = - \sum_{i=1}^N y_i^{mask} \log p_i^{mask} \quad (7)$$

Finally, the total loss function for joint training is composed of three parts:

$$L_{RKB} = \alpha L_{order} + \beta L_{rot} + \gamma L_{mask} \quad (8)$$

where the formulations of  $L_{order}$  and  $L_{rot}$  can be found in Equation 4 and 5.

**Auto Encoder (AE)** Auto Encoder (Schmidhuber, 2015) is a classical neural network architecture for learning compressed features from unlabeled data. The standard framework consists of an encoder  $E$  for condensing information and a decoder  $D$  for reconstructing the original input. As derivatives of Auto Encoder, most generative pretext tasks strive to perform diverse transformations to the input and force the network to recover the original data. To compare with these transformation-based generative SSL, we adopt a primary reconstruction task using original data as the input for Auto Encoder. Take  $x$  as the input, then the loss function is expressed as:

$$L_{AE} = \|x - D(E(x))\|_2 \quad (9)$$

**Model Genesis (MG)** Based on AE, Zhou *et al.* (Zhou et al., 2021b) proposed a SSL framework called “Model Genesis”. In Model Genesis, four strong transformations are randomly applied to the original medical image to generate the input, including the non-linear transformation, local-shuffling, out-painting and in-painting. Let  $\mathcal{T}$  denote the transformations for  $x$ , the objective function can be formulated as:

$$L_{MG} = \|x - D(E(\mathcal{T}(x)))\|_2 \quad (10)$$

**PCRL** As a combination of contrastive and generative SSL, PCRL (Zhou et al., 2021a) is proposed to learn more robust representations. One important innovation is that the generative pretext task recovers a transformed input with a given indicator vector instead of the fixed original input, which can encourage the network to encode richer information. In addition, a mix-up strategy is adopted to restore diverse images. Because of the great complexity of this composite task, we would not list the specific optimization functions here.

**SimCLR** The key idea behind contrastive learning is to maximize the similarity of positive pairs and the dissimilarity of negative pairs in the embedding space. Therefore, the mining scheme of positive and negative pairs is a crucial component in contrastive learning-based methods. In SimCLR (Chen et al., 2020a), given a batch of samples  $x_i, i = 1 \dots N$ , two augmented views of one image is regarded as a positive pair  $(x_i, x_i^+)$  while the other different images  $(x_i, x_j), i \neq j, i, j = 1 \dots N$  are exploited as negative pairs. The common InfoNCE loss (Oord et al., 2018) for contrastive learning is defined as:

$$L_{SimCLR} = -E_x[\log(\frac{\exp(g(x)^T g(x^+))}{\exp(g(x)^T g(x^+)) + \sum_{j=1}^{N-1} \exp(g(x)^T g(x_j))})] \quad (11)$$

in which  $g(\cdot)$  represents the corresponding embedding in the network.

**BYOL** Different with traditional contrastive learning methods that require a large number of negative samples for effective learning, BYOL proposed by Grill *et al.* (Grill et al., 2020) discards negative sampling and only relies on the positive-pair learning. Its architecture is composed of an online network and a target network, where the former is updated normally by gradient decent and the latter is updated by exponential moving average of the online network parameters. Two augmented views  $(x, x^+)$  of one image are passed to online and target network respectively to obtain the embeddings  $(g_o(x), g_t(x^+))$ . For a positive pair, the online network is trained to predict  $g_o(x)$  close to the embedding from target network  $g_t(x^+)$ . The loss function for BYOL can be formulated as:

$$L_{BYOL} = \|(g_o(x) - g_t(x^+))\|_2 \quad (12)$$

### 3.3. Medical datasets and tasks

We present all the computed tomography (CT) datasets that were used as downstream tasks in previous SSL works in Table 2. According to the rank of published numbers, we selected the top three datasets: LiTS, LUNA2016 and LIDC-ICDR, two of which are for the segmentation task and one for the classification task. Note that the training data in MSD-Liver (Antonelli et al., 2022) is from LiTS but its annotations additionally contain the delineation of liver tumour. For simplicity, we use LiTS for liver segmentation and MSD for liver-tumour segmentation, though they are composed of the same CT volumes. Following (Zhou et al., 2021b), we adopt 623 Chest CT scans in LUNA 2016 for pretraining as well and configure the same training and test protocols for the selected target datasets, giving rise to three target tasks called LCS, NCS and NCC. To avoid the test-image leakage between proxy and target tasks, the 623 chest CT scans are the remainder of the LUNA2016 apart from the test set for NCC.

### 3.4. Fair Comparisons and Reproducibility

Based on the benchmarking framework, a comparison of different methods with the same setting is mandatory in a paper. In the field of SSL, many works compared the results of a baseline trained from scratch (FS) and other SSL methods in their own settings. Yet, to our knowledge, the comparison results can be biased due to the study settings.

**Table 3. Comparison of different methods on various target tasks.** Here “NCS” denotes the lung nodule false positive reduction in LUNA 2016 dataset, “NCC” denotes the lung nodule segmentation in LUNA dataset and “LCS” denotes the liver segmentation in LiTS dataset. For NCC, we evaluate the Area Under the Curve (AUC) scores. For NCS, we report both the Dice coefficient scores (DSC) and the mean Intersection over Union (mIoU) with thresholds from 0.5 to 0.95. Note that “mIoU” stands for the average mIoU for the foreground class and background class (used in Zhou *et al.* (2021b)), while “mIoU+” is only for the foreground class. For LCS, we report the DSC and IoU.

Pre-training	Method	NCC		NCS		LCS	
		AUC (%)	DSC (%)	mIoU (%)	mIoU+ (%)	DSC (%)	IoU (%)
From scratch	Random init (He <i>et al.</i> , 2015)	98.53	73.79	80.86	62.58	93.83	88.50
Predictive SSL	ROT (Taleb <i>et al.</i> , 2020)	99.32	73.25	80.64	62.15	94.49	89.65
	RPL (Taleb <i>et al.</i> , 2020)	99.29	<u>76.10</u>	81.36	63.51	<u>94.86</u>	<u>90.18</u>
	Jigsaw (Taleb <i>et al.</i> , 2020)	98.64	75.23	81.90	64.66	94.36	89.42
	RKB (Zhuang <i>et al.</i> , 2019)	<u>99.41</u>	74.22	80.88	62.61	<u>94.93</u>	<u>90.43</u>
	RKB+ (Zhu <i>et al.</i> , 2020)	98.88	74.31	80.82	62.51	<b>95.46</b>	<b>91.41</b>
Generative SSL	AE	97.76	74.26	81.15	63.17	93.77	88.92
	MG (Zhou <i>et al.</i> , 2021b)	98.01	75.69	<u>82.13</u>	<u>65.08</u>	94.24	89.17
	PCRL (Zhou <i>et al.</i> , 2021a)	98.97	75.60	81.97	64.55	93.87	88.56
Contrastive SSL	SimCLR (Chen <i>et al.</i> , 2020a)	99.29	75.96	82.00	64.82	94.56	89.74
	BYOL (Grill <i>et al.</i> , 2020)	<b>99.52</b>	<b>76.13</b>	<b>82.27</b>	<b>65.37</b>	94.43	89.56

One particular phenomenon is that an SSL approach might show a significant performance improvement in the setting of a paper but a marginal gain in the setting of another paper even on the same source and target datasets. For example, in a setting with LUNA as the source dataset and LiTS as the target dataset, MG outperforms nearly 5% than FS in IoU score in (Zhou *et al.*, 2021b) while only 0.6% than FS in dice score in (Zhou *et al.*, 2021a), leading to confusion about the validity of MG.

Another common experiment in related papers is to compare the performance of FS and SSL methods using the varying percentage of labelled training data in the target task. We find that the significant performance gain from SSL pretraining only occurs when exploiting less than 50% of the labelled data. When label utilization attains 100% during fine-tuning, the performance improvement from SSL pretraining is basically less than 1% unit (Tajbakhsh *et al.*, 2019; Tao *et al.*, 2020a; Zhou *et al.*, 2021a; Taleb *et al.*, 2020) or even negative (Tao *et al.*, 2020a; Taleb *et al.*, 2020). This raises the suspicion that the benefits from SSL-based transfer learning in the small-scale labelled training dataset are due to the over-parametrization of standard models rather than meaningful feature reuse, as claimed in (Raghu *et al.*, 2019).

The aforementioned confusions can be attributed to inconsistent settings and weak baselines. To make the results more convincing and offer a fair comparison, we establish a public code framework on PyTorch and reproduce all selected methods across three target datasets with the same setting in each target task. Due to the small scale of medical image datasets, we make full use of annotations in target tasks without any annotation dropping. Each method was trained multiple times and the average results are presented in Table 3. Notably, our baselines (FS) consistently surpass previous implementations in (Zhou *et al.*, 2021b,a) (even with the proposed SSL methods), thus ensuring the performance reality and validity of different SSL approaches.

**Source code, configuration files, and the supplementary material are available at <https://github.com/chuyan99/Medical-SSL>.**

### 3.5. Preliminary analysis of different SSL methods

Our reproduced results in Table 3 first provide a comparison of all the types of SSL pretraining, including predictive, generative and contrastive SSL. Unlike results in previous SSL literature where their proposed SSL method can always prevail over others in various target datasets, we find that no single method is able to dominate in all target datasets. This new finding indicates that

there are a number of practical factors we have to consider for a specific target task to benefit from SSL pretraining, far beyond the design of a pretext task itself. In specific, these factors may include but not limited to the characteristics of upstream and downstream medical data (i.e. class imbalance), effective implementations of SSL tasks, useful combinations with other commonly-used training policies for deep learning.

#### 4. Data Imbalance

In clinical examinations, the number of disease subjects is always far less than normal subjects, naturally leading to heavy "data bias" in medical datasets. This poses great challenges for deep learning models since typical supervised training based on imbalanced data annotations inevitably makes the model overfit to frequent classes and underperform in rare classes. As SSL learns richer features from the inherent information of data, the pretrained model can leverage label-irrelevant-but-transferable features to classify samples instead of only relying on the imbalanced annotations. Due to this, a meaningful question arises:

*How does SSL pretraining affect class-imbalanced learning?*

In this section, we systematically investigate the effect of SSL algorithms on class-imbalanced downstream tasks. We first construct a simple theoretical model to obtain basic intuitions on how class imbalance affects the downstream learning process. Base on theoretical motivation, we design comprehensive experiments to confirm the theoretical insights.

##### 4.1. Theoretical Motivation

In previous works, (Yang and Xu, 2020) has proved that semi-supervised training and self-supervised training can advance class-imbalanced learning. However, their theoretical discussion is based on the ideal assumption that the class priors are balanced, or that the underlying imbalance of unlabeled data does not affect the representation distribution. In this work, we further take into consideration the possible impact of biased priors and unlabeled data on the embedding distribution. Regardless of the complexity of explaining a CNN model, an effective simplified model is tailored toward exploring how SSL act in pattern recognition.

Consider a simple binary classification problem with the data generating distribution  $P_{XY}$  being a mixture of two Gaussians as the target task. Let label  $Y = +1$  and  $Y = -1$  refer to the rare class and major class, which contribute to the ratio of prior probabilities  $0 < \lambda = \frac{P(Y=+1)}{P(Y=-1)} < 1$ . We consider the case where unlabeled data  $\{\tilde{X}_i\}, i = 1, \dots, M$  (potentially also imbalanced) and labelled data  $\{X_j, Y_j\}, j = 1, \dots, N$  from  $P_{XY}$  constitute a pretraining dataset  $D_{up}$  and a target dataset  $D_{down}$ , respectively. We assume that a self-supervised proxy task learns a representation  $Z = \phi(X)$  from  $D_{up}$ . According to the superiority of SSL in previous works, it is reasonable to believe that the new feature  $Z$  is better than the raw input  $X$  for semantic recognition even though we might not explicitly know what the transformation  $\phi$  is. Therefore, the target Bayes's decision boundary is determined by  $Z$  on  $D_{down}$ . Intuitively, the inherent similarity of samples can be learned from the visual data themselves rather than only semantic labels. It has been widely acknowledged that a good SSL model should map visually similar images close together in the embedding space, even though the class labels are unseen. (Wu et al., 2018; Saunshi et al., 2019; Liu et al., 2021) With that said, we can assume that  $Z$  conditioned on  $Y = +1$  and  $Y = -1$  follows different Gaussian distributions. Formally,  $Z|Y = +1 \sim N(\mu_1, \sigma^2)$  and  $Z|Y = -1 \sim N(\mu_2, \sigma^2)$ . Note that we ignore the variance difference between two classes for simplicity. The optimal Bayesian classifier can be expressed as  $f(Z) = \text{sign}(Z - \frac{\mu_1 + \mu_2}{2} + \frac{\sigma^2 \ln(\lambda)}{\mu_1 + \mu_2})$ , i.e.  $X$  is classified as  $Y = +1$  when  $f(\phi(X)) > 0$ . Our estimation of  $f$  is composed of two terms:  $\theta_1 = \frac{\mu_1 + \mu_2}{2}$  and  $\theta_2 = \frac{\sigma^2 \ln(\lambda)}{\mu_1 + \mu_2}$ . For the former term, the estimation is naturally constructed as  $\hat{\theta}_1 = \frac{\sum_{k=1}^{N_+} Z_k^+ + \sum_{k=1}^{N_-} Z_k^-}{2}$ , where  $N_+$  and  $N_-$  are the sample size of positive class and negative class in  $D_{down}$  respectively. Then, we have:

**Theorem 1.** Consider the above setup. For any  $t > 0$ , with probability at least  $1 - 2e^{\frac{-t^2}{2\sigma^2} \frac{N_+ N_-}{N_+ + N_-}}$  our estimated  $\hat{\theta}_1$  satisfies:

$$|\hat{\theta}_1 - \frac{\mu_1 + \mu_2}{2}| \leq t \quad (13)$$

**Interpretation 1.** We discuss the estimation of  $\theta_1$  and  $\theta_2$  separately: (1) Theorem 1 indicates that the imbalance of labelled training data affects the chance of obtaining a good estimate of  $\theta_1$  since that  $\frac{N_+N_-}{N_++N_-}$  is maximized when  $N_+ = N_-$ . (2) The second term implies that extreme data imbalance introduces large estimation uncertainty. As all the training data are derived from  $P_{XY}$  in our prerequisite, class prior information is relevant to the unlabeled data as well. Therefore, it is inaccurate to estimate  $\lambda$  with  $\frac{N_+}{N_-}$  especially when the scale of  $D_{up}$  is larger than  $D_{down}$ , leading to non-negligible estimation uncertainty. For large  $\lambda$  ( $0 < \lambda < 1$ ),  $|\ln(\lambda)|$  turns significant so that the term  $\theta_2 = \frac{\sigma^2 \ln(\lambda)}{\mu_1 + \mu_2}$  dominates the decision function  $f$ , thereby magnifying the estimation uncertainty.

We then consider a large  $\lambda$ , i.e. there is less class imbalance in upstream and downstream data. Based on the understanding in Interpretation 1, we still have a high probability of getting an accurate estimate of the optimal classifier. We further seek the error rate of such a good classifier. Suppose that the Bayes's decision boundary split the whole feature space into two parts:  $\Gamma_+$  and  $\Gamma_-$ , the error probability of each class can be computed as:  $\epsilon_+ = \int_{\Gamma_-} p(Z|Y=+1)dZ$ ,  $\epsilon_- = \int_{\Gamma_+} p(Z|Y=-1)dZ$ . Then, we can derive the *Chernoff* error upper bound according to (Fukunaga, 2013):

**Theorem 2.** Consider the above setup. Given the ratio of prior probabilities  $\lambda$  and the Bhattacharyya distance of two classes  $\mu(1/2) = \frac{1}{8} \frac{(\mu_2 - \mu_1)^2}{\sigma^2}$ , the error probability of each class of Bayes's classifier satisfies:

$$\begin{cases} \epsilon_+ \leq \frac{1}{\sqrt{\lambda}} e^{-\mu(1/2)} \\ \epsilon_- \leq \sqrt{\lambda} e^{-\mu(1/2)} \end{cases} \quad (14)$$

**Interpretation 2.** The Theorem 2 reveals several interesting aspects: (1) The prior probability ratio  $\lambda$  is crucial for the performance of classifier. (2) SSL methods improves the rare class more than the major class. For a supervised learning method, the raw input  $X$  is directly involved in Bayes's decision. Let  $X|Y=+1 \sim N(\mu'_1, \sigma'^2)$  and  $X|Y=-1 \sim N(\mu'_2, \sigma'^2)$ , it is easy to verify the upper bound  $B$  of error rate:  $B(\epsilon'_+) = \frac{1}{\sqrt{\lambda}} e^{-\mu'(1/2)}$ ,  $B(\epsilon'_-) = \sqrt{\lambda} e^{-\mu'(1/2)}$ . In the case where a SSL method achieves lower error rate than the supervised method, we have  $\Delta = e^{-\mu(1/2)} - e^{-\mu'(1/2)} < 0$ . Apparently,  $\frac{1}{\sqrt{\lambda}} > \sqrt{\lambda}$  when  $0 < \lambda < 1$ . Therefore, the positive error rate is reduced much more than the negative error rate. Precisely,  $\Delta_+ = B(\epsilon'_+) - B(\epsilon_+) > \Delta_- = B(\epsilon'_-) - B(\epsilon_-)$ , in which  $B(\cdot)$  represents the upper bound.

#### 4.2. Results

Inspired by the theoretical analysis above, we conduct detailed experiments to explore how SSL boosts class-imbalanced learning in typical medical tasks, including classification and segmentation.

**Classification** To match the theoretical classification model under the premise that all training data come from the same data distribution, we present an imbalanced classification on NCC dataset, as both NCC and the pretraining data are from the LUNA 2016 dataset. The pretraining data is always fixed, while the target data is sampled differently for exploring the effect of SSL on class-imbalanced learning. Let  $x, y$  denote the input and corresponding label, respectively. In NCC dataset,  $x$  with  $y = 1$  is a true-positive nodule and  $x$  with  $y = 0$  is a false-positive nodule, where the amount of the former is much less than the latter. Following (Cao *et al.*, 2019), we define a variable  $r$  as the ratio between the size of the rarest class and the most frequent class. Then we construct distributions with varying imbalance ratio  $r$  in  $\{0.025, 0.05, 0.0075, 0.1, 0.15\}$  for downstream tasks. For each imbalance ratio, we further adjust the number of training samples  $N$  to  $\{5000, 10000, 150000\}$ . Note that we fix the test set for different dataset variants. Apparently, the performance of a baseline model (training from scratch) is not only related to  $r$  but also  $N$ . Given pretrained SSL models, we fine-tune these models with different downstream training datasets and compare each performance with the corresponding baseline model. Fig 2 shows how the performance improvement attained from SSL algorithms  $\Delta I = \Phi_{SSL} - \Phi_{FS}$  varies over different imbalanced distributions, where  $\Phi = 1 - \epsilon$ . In medical imaging, missing true positive cases is much more costly

than false positive cases. Hence, we report the  $\Phi$  of each class separately and focus on the rare class. We surprisingly observed that SSL pretraining performs poorly (even worse than training from scratch) on extremely imbalanced and relatively balanced cases. Our main observations are concluded as:

- (1) SSL yields a marginal impact on the frequent class (less than 0.5%) compared to the rare class, so the rest of our analysis focuses on the rare class.
- (2) SSL achieves very limited improvement on relatively balanced labelled data with a large  $r$ .
- (3) SSL would impair model performance on extreme imbalanced labelled data with a small  $r$ .

These observations indeed support our theoretical insights. In specific, both (1) and (2) highlight that the benefits of SSL are mainly reflected in the improvement over imbalanced categories, further confirming Interpretation 2. In contrast, the impact of SSL on the frequent class is negligible. The extreme case in (3) is relevant to Interpretation 1, which declares that the inherent data imbalance of pretraining medical data also have a negative effect on the downstream learning, from the perspective that both unlabeled and labelled data naturally obey the same class priors. Here, based on broad experiment results, we attempt to explain the negative effect of SSL under extreme imbalance as: In the SSL pretraining stage, biased training data results in skewed representation learning oriented to frequent samples. This representation offset would be expected to get corrected by downstream supervised fine-tuning, but is instead amplified when the downstream labelled data is so severely biased that it fails to provide profitable supervision signals. Therefore, the cumulative biased representation learning under extreme data imbalance leads to poor performance in the rare category. Except for this extreme case, the labels of the downstream data will be conducive to reliable representation learning even if there remains data imbalance. At this point, SSL can be easily rectified by downstream strong supervision, thus not hindering useful SSL features from working well in downstream learning. These findings suggest that for imbalanced classification tasks we should concentrate more on mitigating the data imbalance problem rather than developing SSL methods for pretraining.

**Segmentation** To explore how SSL methods advance model performance on segmentation tasks, we fine-tune various SSL pretrained models on NCS and MSD dataset, and compare each performance with the corresponding baseline model. In MSD dataset, the liver and tumor can be regarded as the frequent class and rare class, respectively. In NCS task, we found that the predictions always fall into two extremes, either with very high dice or very low dice. As explained in Fig. 3, we treat samples with dice value less than 0.4 as hard samples in the rare category and the remaining samples with dice value larger than 0.4 as easy samples in the frequent category. Fig. 4 suggests that SSL tends to exhibit larger gains on the rare class than the frequent class across two datasets. Such results shows the same trend as the classification task, which reveals the advantage of SSL for improving performance of the rare class.

## 5. Network Architecture

The most prevalent architecture for medical image segmentation is the U-shape network (Ronneberger *et al.*, 2015; Çiçek *et al.*, 2016), consisting of a down-sampling encoder, a symmetric up-sampling decoder and skip connections. As a pixel-wise classification task, segmentation relies on fine-grained features to localize the region of object (Hariharan *et al.*, 2015). To integrate features at different levels for precise segmentation, skip connections are proposed to bridge the encoder and decoder, which has achieved outstanding performance (Drozdzal *et al.*, 2016). Constrained by the “pretrain-then-fine-tune” paradigm for transfer learning, it is necessary to ensure that self-training adopts the same encoder architecture as downstream medical tasks. As illustrated in Fig. 1, the network head after the encoder varies for different proxy and target tasks. Apart from the indispensable encoder

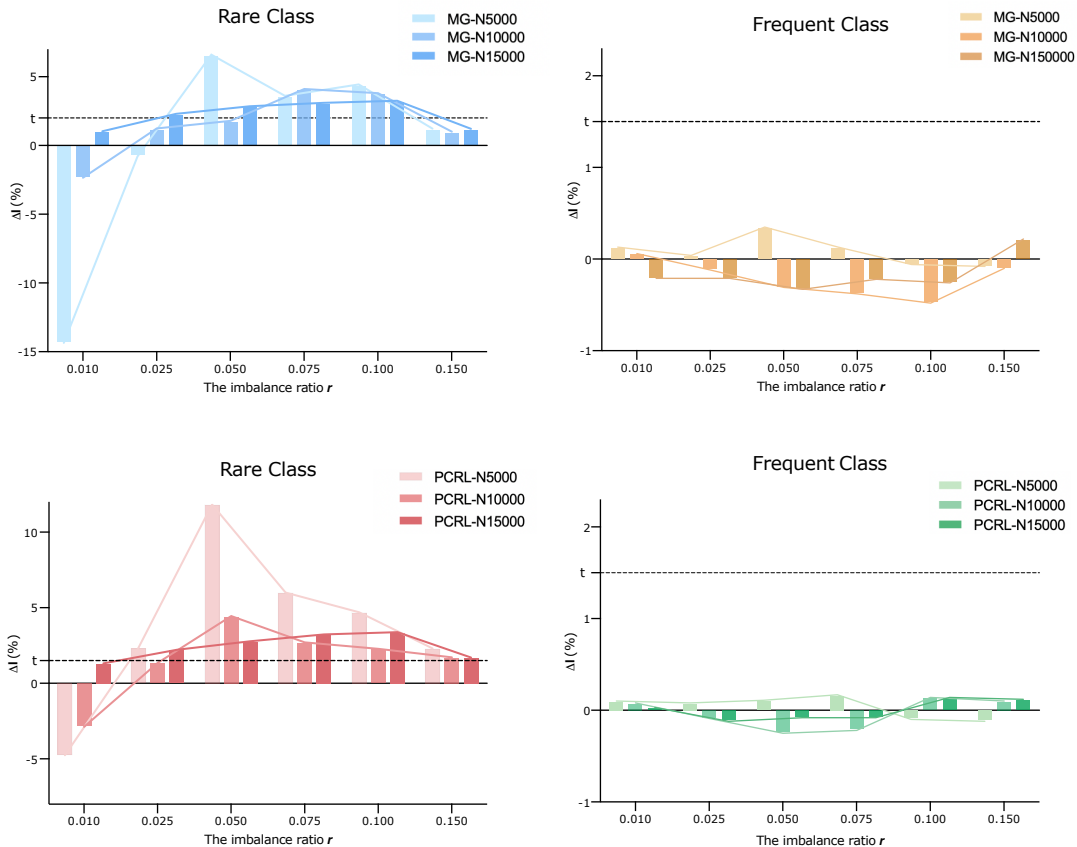


**Fig. 2. Class-imbalanced Classification.** Each pretraining method is tagged as “Method-N\*”. Here, \* is the size of downstream training dataset, and  $\Delta I$  is the error-rate gap between FS and SSL models. We set  $t$  as a threshold representing a significant improvement. As the results show, the improvements from SSL methods are only significant on the rare (positive) class within a range of imbalance ratio rather than the frequent (negative) class.

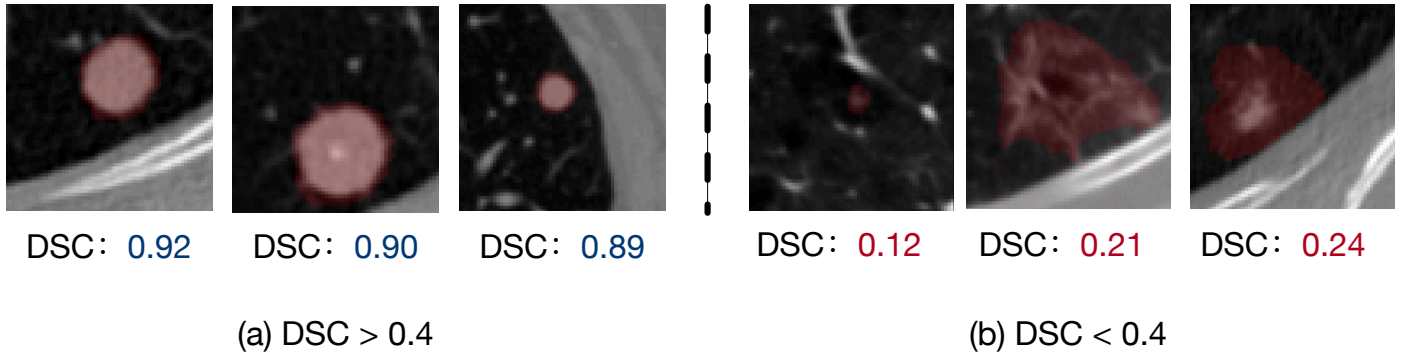


**Fig. 3. Lung nodules with different dice scores (DSC) in NCS.** (a) and (b) display samples with large and small DSC, respectively. The ground truth of each nodule is highlighted in red. We observe that solitary solid nodules often get accurate prediction, while subsolid nodules such as ground-glass or part-solid nodules are difficult to segment. The former nodules in (a) always present isolated, circular and high-density shadows, which are homogeneous; The latter nodules in (b) exhibit mutable forms, which are heterogeneous. Hence, we regard the former as a uniform and frequent class, while the latter is assigned to rare classes.

reuse, the transferring of pretrained decoder’s parameters is also involved in previous papers. For instance, Tao *et al.* (Tao *et al.*, 2020a) claimed that the decoder pre-training alleviates the negative influence of randomly-initialized decoder in the medical image segmentation task. However, this claim remains unsubstantiated, leading to the confusion about the up-to-downstream adaptation schemes. For effective SSL implementations, we investigate the influence of different modules in the U-shape architecture during transfer learning, seen in Fig. 5, as well as the parameter fine-tuning strategy.

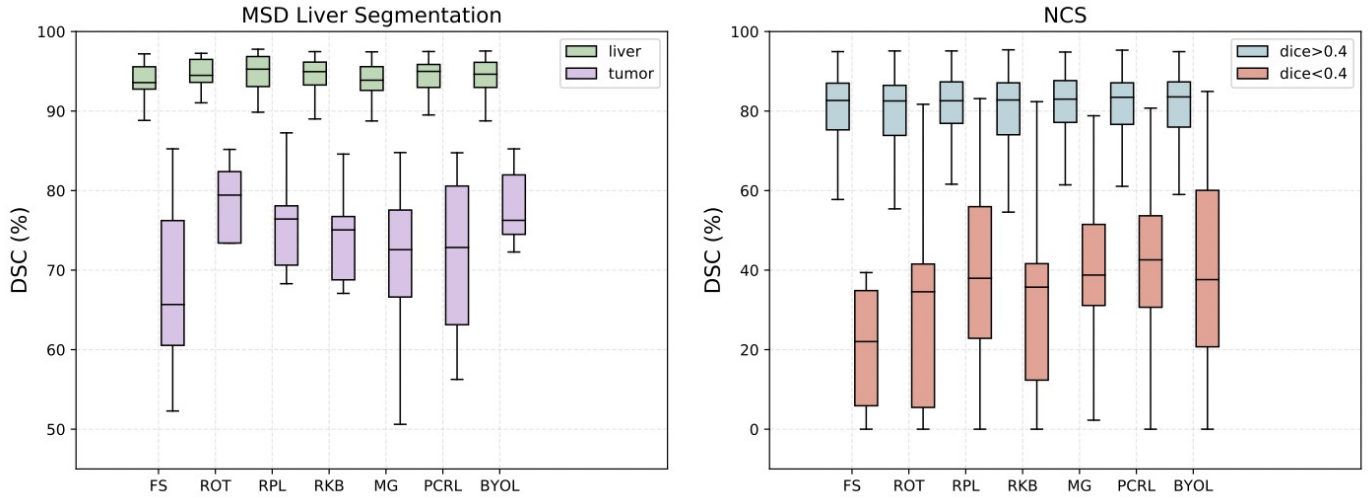


**Fig. 4. Class-imbalanced Segmentation.** We evaluate performance via Dice coefficient score (DSC) for the rare and frequent classes, respectively. Clear improvements from SSL methods are only noticeable for rare classes rather than frequent classes.

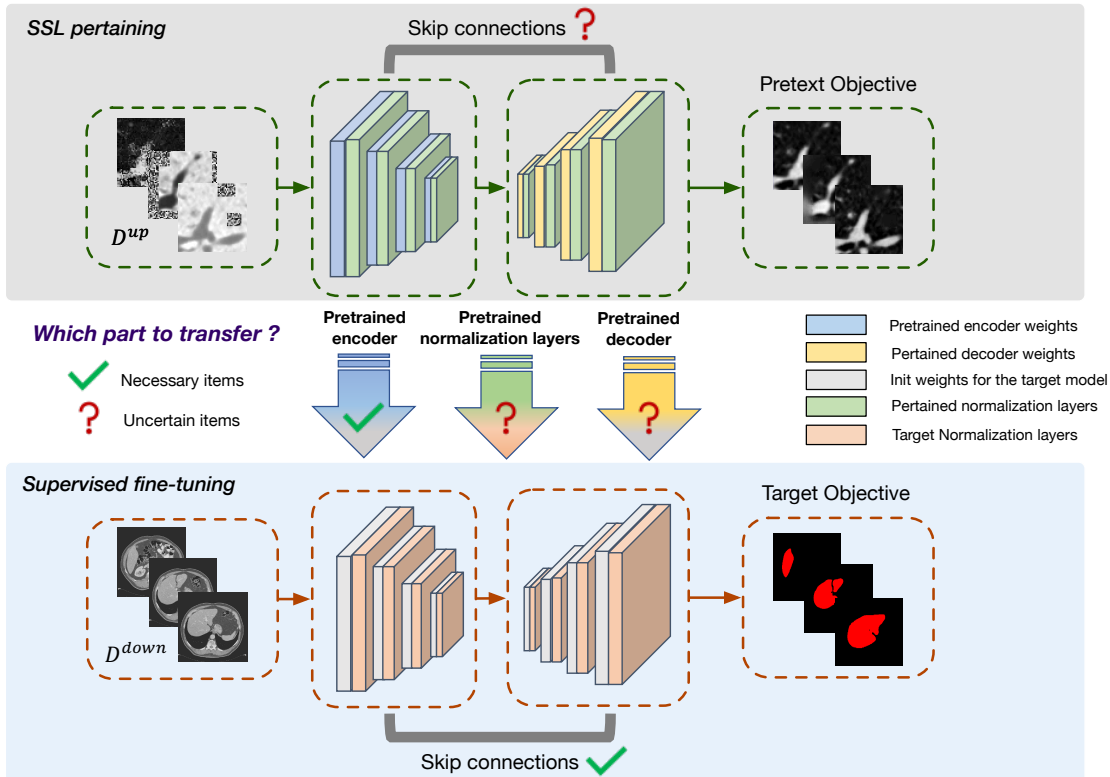


**Fig. 5. Different modules in the SSL pretrained network to be explored to transfer or not.** We illustrate several architecture-related issues during the fine-tuning stage.  $D_{up}$  and  $D_{down}$  represent the training data for solving the pretext task and downstream task, respectively. The remarkable domain difference between  $D_{up}$  and  $D_{down}$  and the objective difference between the pretext and the target task suggest demand for effective weight transfer schemes.

### 5.1. Different modules in the U-shape architecture

To enable the reuse of pretrained parameters, reconstruction-based SSL methods always adopt the same U-shape architecture as medical segmentation tasks. However, we argue that the U-shape architecture with skip connections that are particularly designed for segmentation might be sub-optimal for generative pretext tasks. As the encoder and decoder serve different functions in solving a task, we are also concerned about the roles they play when transferred to target tasks. In specific, different parts of the model

**Table 4. The effect of each module in the U-shape architecture.** For each reconstruction-based SSL method, we first evaluate the performance in target tasks when using separately pretrained encoder, decoder and both. Note that we use dice score as the performance metric for both NCS and LCS, and AUC score for NCC. Then, we re-train each SSL model without the skip connections in the U-shape architecture and report its downstream performance.

Model	Architecture			Pretext task	Target task		
	w/o encoder	w/o decoder	w/o skip		MAE	NCS	LCS
Model Genesis	✓	✓	✓	0.0053	75.69	94.24	98.01
					75.70	94.08	—
					74.77	93.60	—
PCRL	✓	✓	✓	0.0095	77.09	94.72	99.00
					75.59	93.83	98.97
					74.02	93.25	—
				0.0402	74.43	93.56	—
					74.30	93.18	98.34

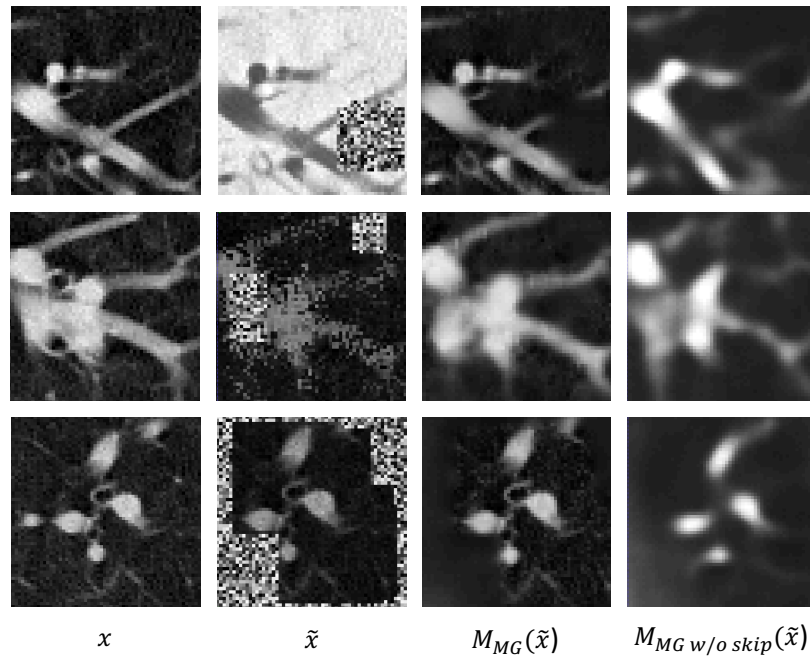


**Fig. 6. Restored images from the pretrained models.** From left to right, the original images, the input images deformed via the MG method, the restored images by the typical MG model and the reconstructed images by the MG model without skip connections.

have different impacts on downstream tasks, and understanding these effects will facilitate the selection of which part to transfer. Thus far, the role of each component in the network architecture is still less explored. In this section, we systematically analyze the impact of encoder, decoder and skip connections on transfer learning by thorough experiments. Accordingly, we transfer different parts of models pretrained by reconstruction-based pretext tasks to various downstream tasks and report the performance in Table 4. In addition, we display the reconstruction error of SSL models on the validation set as a proxy for the difficulty of a pretext task.

**The decoder has the risk of over-fitting to the reconstruction task, thus offering little benefits for downstream tasks.** For the MG method, the model with a randomly-initialized decoder achieve comparable performance to the pretrained decoder, while the absence of the pretrained encoder results in noticeable performance degradation. On the one hand, this overturns the declaration in the previous work that pretraining decoder provides a huge boost on target performance (Tao *et al.*, 2020a). We argue that the

advantages of the designed SSL task might come from better representations in the pretrained encoder instead of the decoder. In the generative SSL, the encoder aims to learn valuable rich anatomical information and the decoder has to recover pixel values from encoded representations. Thus, the decoder could risk the overfitting to local visual details of volumes. Although such fine-grained features are useful for localizing regions of interest, pixel classification relies more on high-level semantic features. Consequently, the features in the decoder might not be well transferable for segmentation. Nonetheless, PCRL avoids overfitting visual details by introducing contrastive learning and transformation-conditioned reconstruction into the pretext task, thereby providing a more valuable decoder for transfer. On the other hand, the poor performance of only transferring decoder prove that it is not feasible to initialize parameters in a truncated manner by randomly initializing previous layers (encoder) and transferring pretrained parameters after these layers (decoder). To ensure the validity of the self-supervised learned representations, the transferred parameters should not be disconnected.

#### Removing the skip connections in self-training could mitigate the over-fitting of the network to reconstruction details.

It has been commonly accepted that the skip connection in the U-shape network intends to assemble high-resolution and low-level features from the encoder layers with the decoder layers for more precise outputs for segmentation tasks. As for reconstruction proxy tasks, this contracting path can hurt the model generalization since the network would easily restore medical volumes by conserving the fine-grained details from the encoder layers rather than learning semantic features. As shown in Fig. 6, the restored images from the MG model retain almost all the subtle details of volumes, thus exhibiting a considerable high reconstruction quality. Then, we remove the skip connections in the U-shape network for proxy tasks and find that such model only restores the major structures. It is therefore reasonable to attribute these minor details in MG restored images to the skip connections. However, what really matters is the representative features contributing to the subsequent semantic task rather than the performance of the pretext task itself. If most of the information can be easily transmitted from the front layers to the decoder, the encoder will have little incentive to encode valuable features for the decoder. Instead, removing the skip connections when solving pretext tasks would force the network to extract high-level anatomical features. The results in Table 4 illustrates that removing the skip connections in MG method leads to worse reconstruction quality on the pretext task, but better performance on various downstream tasks. Nevertheless, removing the skip connections is detrimental when the pretext task is hard enough, e.g. PCRL. In specific applications, it is necessary to consider the difficulty of pretext task to decide whether to take measures to prevent the potential overfitting issue.

#### 5.2. Normalization Layer

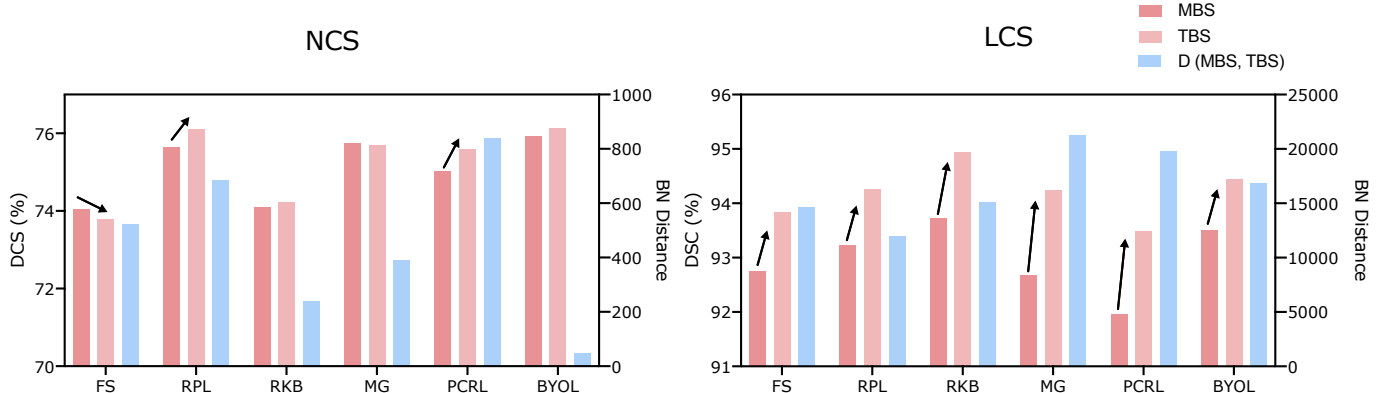


**Fig. 7. Comparison of different BN statistics.** For each method, the predictions are obtained by Mixed BN statistics (MBS) and Target BN Statistics (TBS), respectively. We also report the BN distances of TBS and MBS.

We notice that current SSL studies have neglected an important issue that the transfer might be hurdled by the distribution shift between proxy and downstream tasks. This shift is caused by two main factors: (1) the data-domain gap from the upstream input data to the downstream input data, e.g. different anatomical structures, diverse modalities and transformations applied to original data in proxy tasks; (2) the feature-domain gap due to different training objectives of SSL and FSL. It has been proved that the data domain traits is included in Batch Normalization (BN) statistics (Li *et al.*, 2016). In the field of Domain Adaptation, the importance of separating BN layers for different domains has been emphasized frequently (Chang *et al.*, 2019). Motivated by this, we attempt to seek an appropriate BN adaptation policy for SSL-based transfer learning.

During the fine-tuning stage, all the layers are initialized with pre-trained parameters except the final network head such that the distribution statistics in BN layers merge the target data with the historical data used in pretraining. In case the mixed data distribution would be detrimental to the target task performance, BN statistics are required to obey the target data distribution. But if we simply drop the historical BN buffers in the pretrained model and randomly initialized these BN layers, the fractured reuse of weights can easily lead to failed transfer. Therefore, we recommend to re-collect the normalization statistics of the target data to normalize features of the target domain in the test stage.

Following (Zhou *et al.*, 2022), we compute the distance between the mixed and target BN statistics (MBS and TBS for short) as a quantitative measurement of distribution shift. The BN distance function can be written as:

$$Dist(MBS, TBS) = \sum_{l=1}^L \|(\mu_{mixed}^l - \mu_{target}^l)\|_2^2 + \|(\sigma_{mixed}^{l2} - \sigma_{target}^{l2})\|_2^2 \quad (15)$$

where  $(\mu_{mixed}, \sigma_{mixed}^l)$  and  $(\mu_{target}, \sigma_{target}^l)$  are the corresponding statistic values in BMS and TBS. To obviate the influence of decoders or network heads, we only measure the BN distance of encoder layers  $\{1, 2, \dots, L\}$ .

**Mixed BN statistics usually induces performance degeneration at a large distribution distance so that recollecting the target BN statistics for inference is necessary.** Fig. 7 compares the performance of MBS and TBS in two segmentation tasks. The results demonstrate our hypothesis that TBS outperforms MBS by visible gaps when the distribution distance is large. For NCS, the same upstream and downstream data means that the data-domain gap is minimal. Still, the representation gap between proxy and target tasks or the data-domain gap between training and test data might account for the small performance difference of MBS and TBS. For most of the SSL methods, the performance of MBS and TBS do not clearly favor one over the other. For LCS, the upstream and downstream CT volumes are from chest and abdomen respectively. Consequently, the distance between MBS and TBS in LCS are much larger than that in NCS. In this case, it is necessary to discard the mixed statistics and gather the target statistics for predictions. Otherwise, the large distribution shift usually results in significant performance degeneration. Overall, we believe that adopting TBS in specific target tasks is a reliable way to avoid the potential risk of mismatched BN statistics.

### 5.3. Fine-tuning strategy

Given a SSL pretrained model, how the parameters are reused determines whether meaningful SSL features are transferred well for solving downstream tasks. Throughout related works, there are mainly three choices of fine-tuning the pretrained model to target tasks: fixed (Goyal *et al.*, 2019), warmup (Taleb *et al.*, 2020), and full fine-tuning (Zhou *et al.*, 2021b). The fixed way is to freeze the encoder and fine-tune the head (decoder stacks or fully-connected layers) for the target task. In contrast, the full way is to fine-tune all the weights with a relatively small learning rate. As a neutral to the above two ways, the warmup way first fixed the encoder for a few epochs and then execute the full fine-tuning. We first exclude the fixed way as the fixed weights learned from a proxy task are hardly able to perform well in the target task, especially when there exists a distinct up-downstream domain gap.

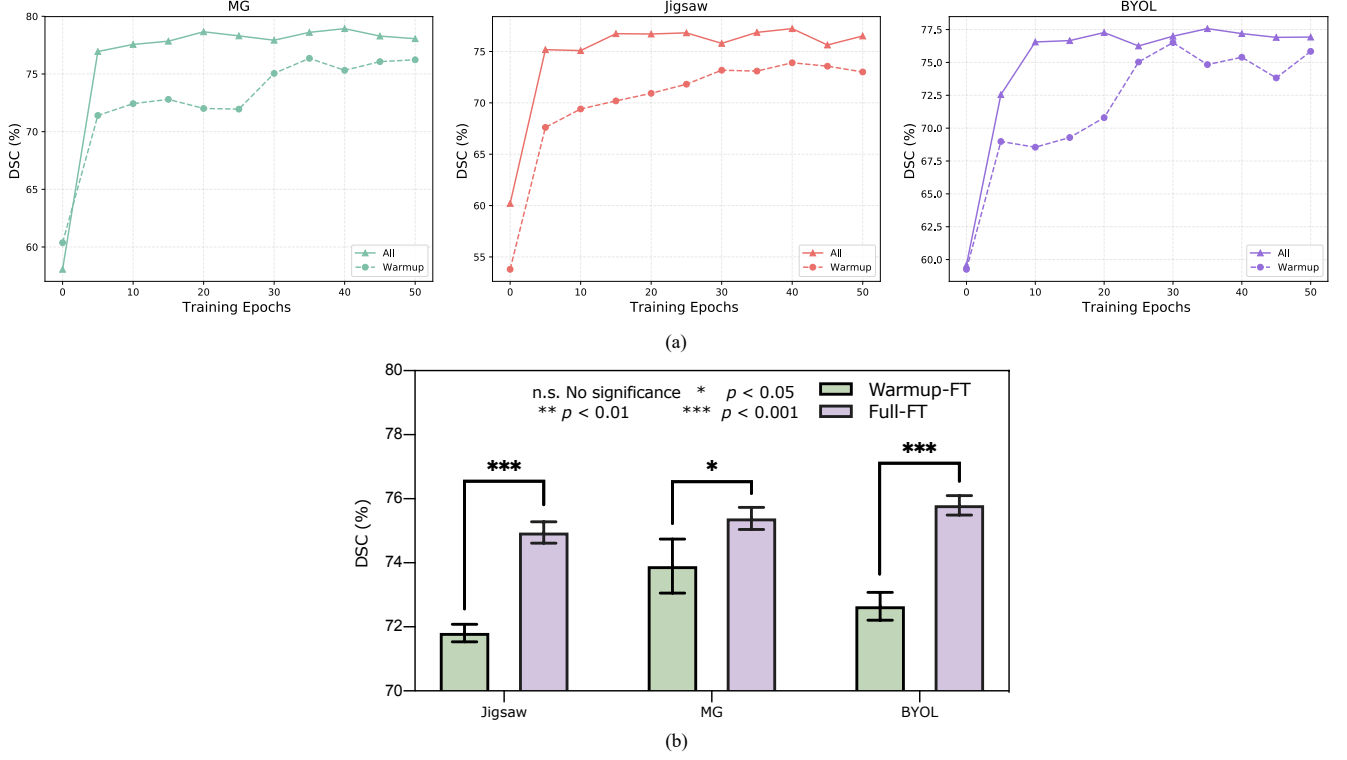


**Fig. 8. Results of different fine-tuning schemes in (a) the validation set of NCS and (b) the test set of NCS**

Then, we investigate the warmup and full ways for transfer learning. We select three representative pretext tasks from predictive, generative and contrastive SSL methods: Jigsaw, MG and BYOL.

**Full fine-tuning is more advantageous than warmup fine-tuning for SSL-based transfer learning due to the essential gap between self-training and downstream tasks.** Our experiments present a consistent outcome that the full fine-tuning is superior to the warmup fine-tuning among three SSL tasks. The validation performance over training epochs with different fine-tuning schemes is shown in Fig. 8 (a). It can be observed that the performance of the warmup scheme is noticeably behind the full scheme from the start of the fine-tuning stage across three SSL methods. The test results in Fig. 8 (b) also show the same tendency that the full scheme significantly exceeds the warmup scheme. It is worth mentioning that the decline caused by warmup fine-tuning is the smallest in the generative model, probably because the reconstruction task is closer to the segmentation task intrinsically (both more concerned with fine-grained features at pixel level) than the other two. Therefore, we recommend full fine-tuning with a small learning rate instead of fixed pretrained parameters for SSL techniques.

## 6. Pretext tasks

With the rapid development of SSL, more and more interesting pretext tasks are being discovered. These works focus on presenting a new proxy task and proving its priority over existing methods, but lack a more detailed comparison with other SSL methods, such as the effective scope of each method. Actually, our reproduction of diverse SSL methods in Table 3 has shown that no single SSL method dominates in all target tasks, indicating that a universal SSL pre-training remains infeasible. Thus, researchers have to confront a fundamental question below:

*How to implement an effective SSL pretraining from a variety of SSL approaches to facilitate a specific target task?*

In this section, we seek to answer this question in three steps. In the first step, we analyze the adaptation performance from

different types of pretext tasks to downstream tasks and summarize several guidelines for selecting an appropriate SSL task. Then, we discuss the influence of data processing for performing predictive SSL. Finally, we conduct a feature-level comparative analysis on diverse SSL tasks to account for their differing performance on target tasks.

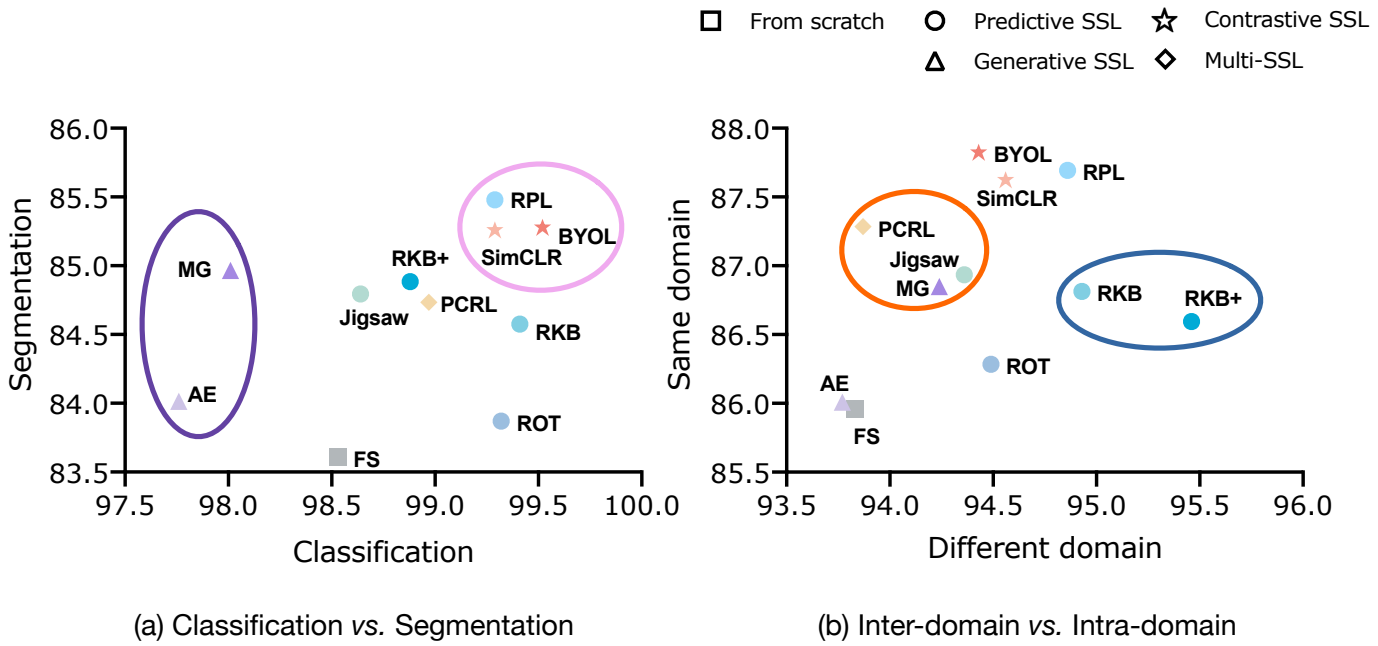


**Fig. 9.** Comparison of different methods in terms of target tasks and the up-downstream data domains. (a) shows the performance of methods in regular medical recognition tasks, namely classification and segmentation tasks. Here, we treat the average dice value of NCS and LCS as the measurement of the segmentation task. (b) draws the behaviours of methods in inter-domain and intra-domain transfer learning. Since the NCC and NCS data are both from the same domain in pretraining dataset, we treat the average value of NCC's AUC score and NCS's dice score as the measurement of intra-domain transfer. As for the inter-domain transfer, the dice score is measured in LCS.

### 6.1. Selection of Pretext Tasks

It is necessary to discuss the behaviours of different SSL tasks in different downstream tasks. For a specific target task, we put forward several considerations when selecting a pretext task. The followings are our discussions and suggestions:

**The generative SSL methods underperform in the classification task.** As drawn in Fig. 9(a), the generative SSL lags far behind other types of SSL in classification. A possible explanation may be the different attention between reconstruction to semantic classification, with the former focusing more on fine-grained details and the latter preferring high-level representations. In contrast, the predictive and contrastive SSL methods pay attention to the high-level anatomical structures. Therefore, we recommend predictive and contrastive SSL over generative SSL for the classification task.

**Take into account properties of the target task when selecting the pretext task for pretraining.** As a prominent example, predicting rotations is not a viable proxy task for lung nodule segmentation. Since circular lung nodules tend to be rotation invariant, rotation-relevant features should not occupy too much attention of the network. Consequently, rotation-related SSL models consistently perform poorly on NCS. The inferior performance of RKB to Jigsaw also confirms this idea since an additional rotation prediction sub-task is added to RKB compared with Jigsaw.

**For the adaptation with a large data-domain gap between upstream and downstream data (e.g. LCS), it is important to prevent the potential overfitting to the upstream data in predictive or generative SSL.** In Fig. 9(b), we can observe that few predictive SSL and the generative SSL perform poorly in intra-domain transfer learning. In the predictive SSL, the Jigsaw

**Table 5. The input size of different tasks. In the upstream tasks, the number after “ROT” and “RPL” stands for the input size in axial (H-W) view. In the downstream tasks, the 0.5 in LCS means that we apply a 0.5x downsampling to the inputs, due to the limited GPU memory.**

Task	Input size (H×W×D)
Upstream	ROT-48
	ROT-64
	ROT-128
	RPL-48
	RPL-64
	RPL-96
Downstream	NCC
	NCS
	LCS
	48×48×32
	64×64×64
	128×128×64
	48×48×32
	64×64×32
	94×96×32
	48×48×48
	64×64×32
	512×512×(74~987)*0.5

task might be overfitted to the fixed order arrangements that were determined before. In contrast, harder predictive tasks tend to perform better, such as predicting the relative position of two randomly cropped patches or integrating more orthogonal sub-tasks to Jigsaw (RKB, RKB++). In the generative SSL, previous reconstruction task based on the typical U-Net backbone are more likely to learn trivial solutions from the pre-training data (LUNA16), leading to limited transferable performance on LCS. Removing the skip connection in U-shape architecture would mitigate such overfitting issue.

**For blindly choosing, contrastive SSL and RPL could be the go-to solutions for researchers.** From the Fig. 9 above, we can see that SimCLR, BYOL and RPL achieve robust good performance across all target tasks. This reveals promising advantages of contrastive SSL for learning more robust representations in medical imaging compared with other SSL.

## 6.2. Sensitivity of predictive SSL methods with respect to the input size

In a predictive pretext task, the size of input volumes determines the amount of spatial information from which the network extracts features, thus influencing the expressive power of self-supervised learned features. As a crucial hyperparameter for SSL pretraining, the input size adopted in pretext tasks needs to be thoroughly investigated. However, related works (Taleb *et al.*, 2020; Zhuang *et al.*, 2019) only supply a brief description of the choice of input size. To assess the impact of input size on the self-supervised learned features, we pretrain SSL models using cubes of different sizes (see Table 5) and examine them in various target tasks (see Figure 10). Below are our key findings:

**The accuracy of proxy tasks increases as the input size grows.** The logic is that it will be easier for networks to predict transformations with more spatial information available.

**The accuracy of proxy tasks and the performance of downstream tasks are not simply positively correlated.** Specifically, higher accuracy on SSL tasks does not imply better performance on downstream tasks. When the input size is reduced to 48, we suspect that valid SSL features could not be well-learned by the ROT model (At least the RPL model takes two patches as input instead of a single patch). This can explain why the ROT model with small inputs perform bad on both NCS and LCS.

**The sensitivity of input size varies for different SSL methods and target tasks.** For the classification task, the variation caused by varying input sizes is negligible for both ROT and RPL. However, segmentation tasks tend to exhibit distinctive performance for ROT. That is, the ROT pretrained model is very sensitive to the input size of upstream data in segmentation, and it performs best when the input size of upstream data attains the same as the downstream data. In contrast, the RPL pretrained model is robust to the input size.

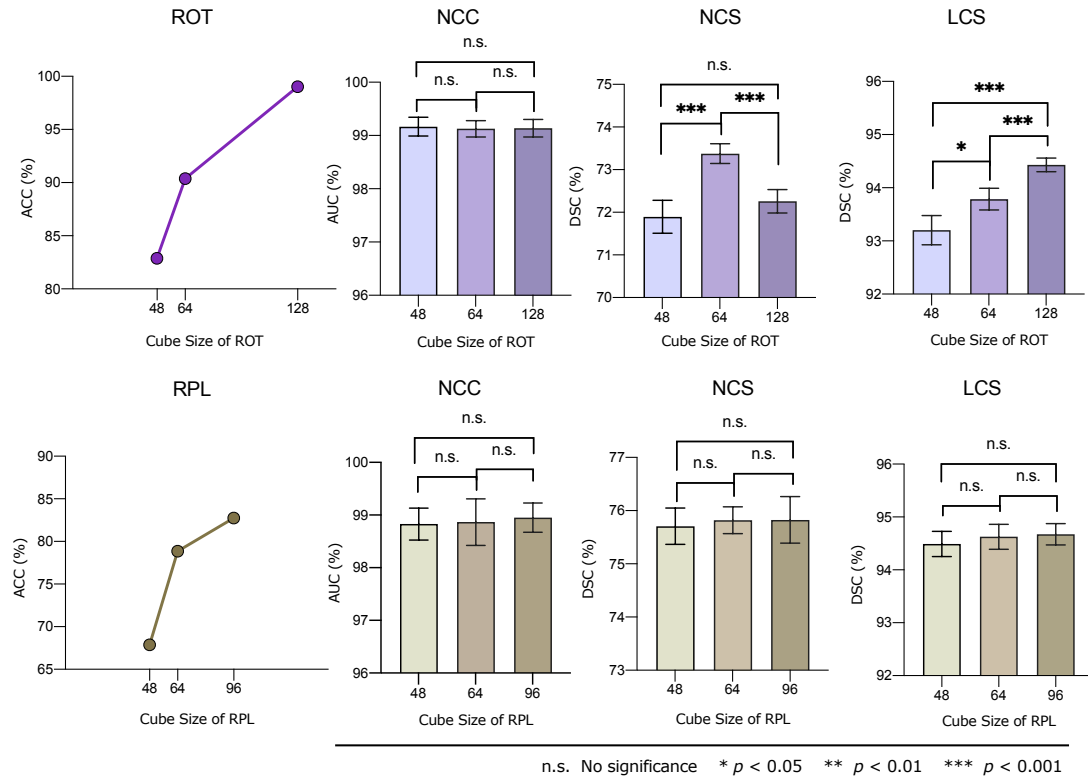


**Fig. 10.** The impact of input size for predictive SSL methods. For pretext tasks, the classification accuracy with regard to varying input size is evaluated on the validation set. For target tasks, we evaluate the AUC score and Dice score for classification and segmentation tasks respectively on each test set.

To prevent the risk of performance degradation caused by transferable features due to sensitivity to inconsistent input sizes, a simple proposal is to keep the input sizes of pretraining and fine-tuning data as close as possible.

### 6.3. Feature analysis of SSL models

Convolutional neural networks are generally considered to extract hierarchical features, where the low/middle layers contain general features and the higher layers extract more task-specific features (Neyshabur *et al.*, 2020; Haghghi *et al.*, 2020). Based on the above understanding, the benefits of transfer learning have been proved to stem from pre-trained low/mid-level feature reuse in target tasks (Neyshabur *et al.*, 2020; Zhao *et al.*, 2020). Now that major applications of SSL methods are still obeying a transfer learning paradigm so that the same conclusion holds for SSL pretraining (Asano *et al.*, 2019; Islam *et al.*, 2021). To access a better grasp of the impact of different SSL pre-trained features on medical imaging tasks, we carry out the following quantitative and qualitative analyses across diverse SSL approaches.

**A. Feature visualization analysis.** To investigate the difference between reused features of various SSL methods for the classification task, we visualize focal regions associated with the network decisions through Gradient-weighted class activation maps (Grad-CAMs). The results of networks trained on NCC dataset with different SSL approaches are shown in Fig. 11. Our observations are as follows:

- The predictive SSL models (ROT, RPL, RKB) look exactly at nodules. Compared to the constrictive activation regions in ROT, RPL and RKB pretrained models pay additional attention to the area adjacent to nodules. The underlying reason might be that these two pretext tasks involve predicting relative positions and therefore demand more context information while ROT pretrained model focuses more on the discriminative structure of objects.

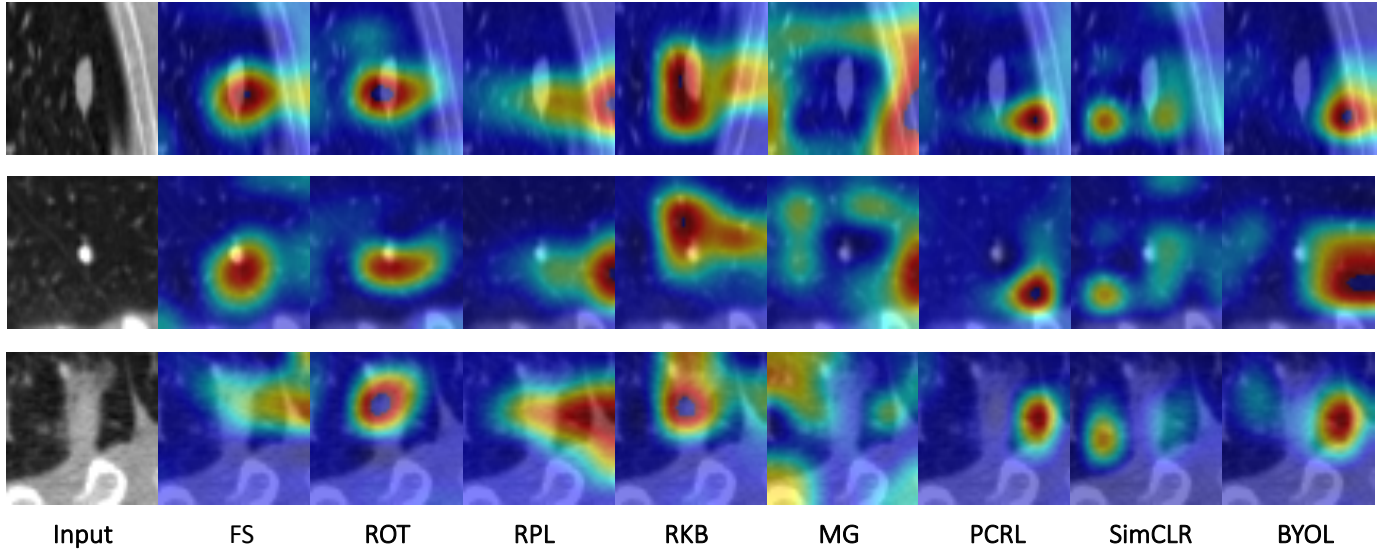


Fig. 11. Grad-CAMs of different SSL methods on NCC. The left column exhibits original images containing lung nodules. The remaining columns shows the corresponding Grad-CAMs by different models.

- The focus of generative SSL models is prone to backgrounds instead of foreground objects. This is reasonable since the reconstruction task is bound to focus on subtle details. Consequently, the reconstruction-based SSL pretraining leads to better performance gains for segmentation tasks rather than classification tasks, as the fine-grained features are more desired for delineating objects.
- Although contrastive SSL models have noticed partial nodules, most of the attention is distracted to surrounding regions. Apparently, such off-focus is caused by the contrastive learning mechanism that depends on maximizing mutual information between positive pairs, whereas a rigorous interpretation remains a mystery.

**B. Feature similarity analysis.** Intuitively, useful pretrained features for downstream tasks would be retained during the fine-tuning process. Thus, the extent of feature reuse can be indicative of the efficiency of a SSL algorithm in downstream tasks. Following (Neyshabur *et al.*, 2020; Taher *et al.*, 2022), we use the Centered Kernel Alignment (CKA) (Kornblith *et al.*, 2019) to measure the feature similarity of the pretrained features and fine-tuned features on downstream tasks. To avoid interference caused by the disparity between upstream and downstream data, we examine the CKA score on NCS and NCC datasets, which are identical to our pre-training data. We extract features from conv1 to conv4 in the encoder of U-Net, denoted as layers 1 to 4, and then pass them to a global average pooling layer to compute feature similarity. We fine-tune each method multiple times and report the average CKA score on each task in Table 6. In particular, we add generative SSL models without skip connections in U-Net and predictive SSL models with varying input size to further investigate the idea in 6.2 and 5.1. We first analyze the trends of diverse SSL methods in general, and then scrutinize the effects of input size and model structure:

- For NCC, it is obvious that the lower features in first three layers are more reusable in predictive SSL pretraining than generative and contrastive SSL pretraining. The middle-feature similarity in the final layer is high in ROT, RKB and BYOL. In fact, it is precisely these three methods that yield the best results in NCC task according to Table 3. As for NCS, the RPL model shows remarkably high feature reuse score at each layer, accounting for the superior performance in Table 3. Similar to NCS, the BYOL model shows higher feature similarity in middle layers than in low layers. Combining the feature reuse and the performance in the downstream tasks, we declare that higher feature reuse is more productive for transfer learning.

**Table 6. Comparison of feature reuse between different SSL methods in two downstream datasets. For each method, we report the CKA similarity score between the pre-trained and fine-tuned model in terms of 4 layers. In each column, the CKA scores above 70% percent are highlighted in bold. The number after “ROT” and “RPL” stands for the input size in axial view.**

Pre-training	Method	NCC				NCS			
		Layer1	Layer2	Layer3	Layer4	Layer1	Layer2	Layer3	Layer4
Predictive SSL	ROT-48	<b>0.954</b>	<b>0.747</b>	0.493	0.292	0.878	0.867	0.758	0.705
	ROT-64	<b>0.944</b>	<b>0.815</b>	<b>0.599</b>	0.243	<b>0.945</b>	0.901	0.872	0.745
	ROT-128	0.688	0.646	0.412	<b>0.611</b>	0.805	0.838	0.833	0.730
	RPL-48	0.805	<b>0.692</b>	0.520	0.174	<b>0.979</b>	<b>0.970</b>	<b>0.956</b>	0.786
	RPL-64	0.815	0.648	0.541	0.197	<b>0.975</b>	<b>0.954</b>	<b>0.952</b>	<b>0.902</b>
	RPL-96	<b>0.823</b>	0.628	0.489	0.280	<b>0.971</b>	<b>0.955</b>	<b>0.965</b>	<b>0.938</b>
	RKB	<b>0.968</b>	<b>0.863</b>	<b>0.706</b>	<b>0.625</b>	0.897	0.905	0.893	0.788
Generative SSL	MG	0.810	0.667	0.506	0.140	0.949	0.912	0.819	0.665
	MG(w/o skip)	0.676	0.680	<b>0.636</b>	<b>0.415</b>	0.891	<b>0.937</b>	<b>0.929</b>	<b>0.826</b>
	PCRL	0.728	0.461	0.171	0.113	0.937	0.863	0.757	0.643
	PCRL(w/o skip)	0.652	0.483	0.320	0.172	0.865	0.888	0.723	0.626
Contrastive SSL	SimCLR	0.598	0.652	0.532	0.383	0.837	0.868	0.862	0.787
	BYOL	0.683	0.665	<b>0.690</b>	<b>0.463</b>	0.882	0.889	0.905	<b>0.837</b>

- Overall, the variation of feature similarity due to input size is evident in ROT but close in RPL across two downstream tasks. This can further explain why the downstream performance is sensitive to ROT method in Figure 10. As an exception, the performance of NCC is robust to ROT. This may be attributed to the fact that the significant improvement in feature reuse score at the last layer of ROT-128 compensates for the poor feature reuse at the first three layers.
- Regarding the U-shaped structure, we discover that removing skip connections in MG significantly increases the reuse rate of higher features, even though it may compromise a bit lower feature reuse rate. This observation solidly confirms our view in 5.1, i.e. removing skip connections suppresses the overfitting issue in the pure reconstruction task. However, PCRL is actually a combination of multiple pretext tasks which might be non-trivial enough to solve. So removing skip connections in PCRL would instead make it more difficult to learn valid transferable features, resulting in less feature reuse.

## 7. Common training policies

Either the experiments in the previous papers in natural image classification (Liu *et al.*, 2021; Yang and Xu, 2020) or our experiments in common medical tasks in Section 4 point to one finding: one of the foremost benefits of SSL pretraining is the performance gain under class imbalance. Regarding SSL as a strategy to tackle class imbalance, we wonder if it could be overlaid with other widely used strategies, including resampling and data augmentation, to achieve better performance. For that purpose, we evaluate the effects of stacking SSL with other strategies in two tasks, NCC and NCS, covering both classification and segmentation tasks.

### 7.1. The additive effect of SSL and resampling.

As a simple yet effective strategy for class-imbalanced learning, data resampling over-samples data from the rare classes or under-samples data from the frequent classes to alleviate class bias (Cao *et al.*, 2019). Following (He *et al.*, 2021), we adopt the

mean resampling schedule for NCC task, i.e. assigning an equal probability for each class to be sampled during training epochs. We consider different class-imbalance settings as in Section 4 by changing imbalance ratio  $r$  and the number of training samples  $N$ . In each setting, we first train a network without any extra strategies as the baseline. Then, we use the mean resampling strategy and SSL pretraining to retrain the network.

Table 7 summarizes the performance gains from data resampling and SSL methods over the baseline on NCC. The AUC and recall scores focus on overall classification and positive class performance respectively. Note that the positive class is the minority class in NCC task. An obvious downside of mean resampling schedule appears for extreme less data in positive class (small  $r$  or  $N$ ). This means that resampling discards a large amount of the data to ensure the equal sampling possibility in both classes, which can lead to overfitting of small remaining portion of the data and thus impair the performance. With increasing number of the positive class, mean resampling schedule tends to exhibit larger gains over baseline. Nonetheless, these gains are limited since the performance seems to saturate when  $r$  and  $N$  is large enough, namely slight class imbalance. Based on the resampling, we further explore the impact of SSL pretraining.

**The combination of resampling and SSL techniques is preferred in severe class-imbalanced and data-poor regimes while solely resampling is preferred in slight class-imbalanced regimes.** As opposed to the poor performance of SSL under extreme class imbalance (small  $r$ ) in Figure 2, we observe that SSL with the resampling schedule can boost task performance significantly. This indicates a complementary effect between SSL and resampling for severe imbalanced learning that SSL can improve the drawback of overfitting to small samples in mean resampling while mean resampling can balance the skewed SSL representation distribution. In scenes with minor data imbalance, however, SSL methods generally have a little effect on the whole performance. Actually, only using SSL pretraining lags behind the mean resampling schedule a lot.

## 7.2. The additive effect of SSL and data augmentation.

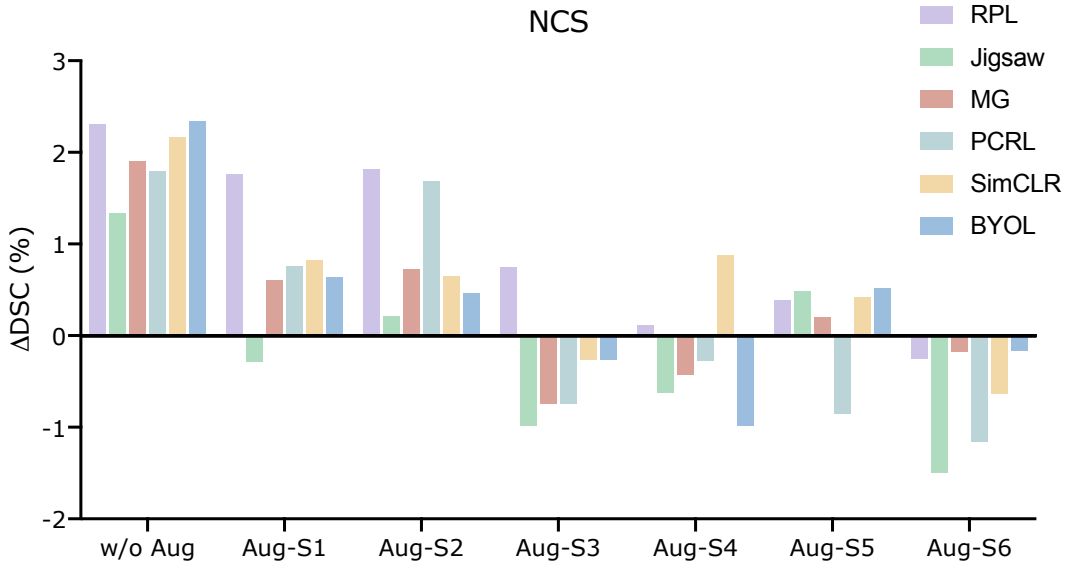


**Fig. 12. The effects of data augmentation on different SSL methods.**  $\Delta$ DSC refers to the difference between a SSL pretrained model and the baseline model in Dice score. The data augmentation degree is increasing from “Aug-S1” to “Aug-S6”.

Data augmentation plays an essential role in training CNNs, involving preventing overfitting and enhancing generalization performance. Additionally, it can mitigate the data imbalance issue by reduce overfitting to the observed samples, most of which belong to majority classes. We employ five compositions of data augmentation with different degrees for NCS task and investigate

**Table 7. The performance gains of different training strategies over the baseline on NCC task. The additional gain of SSL pretraining over merely resampling ( $> 1\%$ ) is highlighted in blue.**

Imbalance Ratio	$N$	Mean-Resampling		+MG		+PCRL	
		$\Delta_{AUC}$	$\Delta_{Recall}$	$\Delta_{AUC}$	$\Delta_{Recall}$	$\Delta_{AUC}$	$\Delta_{Recall}$
$r=0.01$	5k	-4.21	19.10	(+6.10)	1.89 (+13.28)	32.38 (+2.77)	-1.44 (+24.24)
	10k	9.96	37.00	(+12.57)	22.53 (+17.31)	54.31 (+4.93)	14.89 (+22.53)
	15k	17.21	52.66	(+1.96)	19.17 (+17.75)	70.41 (+4.01)	21.22
$r=0.05$	5k	4.14	45.16	(+10.20)	14.34 (+3.93)	49.09 (+2.33)	6.47
	10k	22.94	47.25		22.98	47.01	21.39
	15k	21.05	44.13		21.25 (+8.09)	52.22	19.04
$r=0.1$	5k	-6.20	40.21	(+4.68)	-1.52	34.99 (+2.94)	-3.26
	10k	16.42	47.78		16.12	47.51	16.45
	15k	11.26	47.51		11.53	46.21	9.98

the stacking effect with SSL methods. Table 7 plots the performance gains from SSL methods with different data augmentation policies of increasing strength over the baseline on NCS.

**Strong augmentation diminishes the value of SSL pretraining.** We find that SSL only provides clear improvements without any data augmentation or with a weak data augmentation. But as we increase the strength of data augmentation, the benefit of SSL diminishes. Several SSL techniques even hurts performance when strong data augmentation is applied. We hypothesize that strong augmentations already advance imbalanced learning which might cancel out the gains introduced from SSL pretraining.

## 8. Discussions and Future Directions

### 8.1. The effectiveness of SSL for medical image analysis

Our results in Table 3 suggest that contrastive learning-based tasks exhibit more promising performance, albeit no SSL task always performs best throughout all the medical tasks. For simplicity, we directly apply prevalent contrastive learning frameworks in natural scenes to medical tasks, with a minor modification to ensure overlap between a positive pair. Surprisingly, such models exceed most of the models pretrained with carefully-designed tasks (e.g. PCRL) across all three tasks. As mentioned in Section 2.1, we believe that re-designed contrastive learning for medical images can achieve much better performance. In contrast, different predictive tasks generally show distinct performance across target tasks and the generative tasks tend to be on the tail end. Among these tasks, we find RPL consistently delivers significant improvements over baselines.

From the perspective of task design principles, one intrinsic defect of current predictive and generative SSL tasks requires to be resolved for robust representation learning, otherwise, contrastive SSL would be more reliable. That is, the objective of many pretext tasks is so harsh that even a medical expert cannot accomplish it, which departs the purpose of self-discovering semantically useful information contained in medical images. Two SSL tasks are typical for our discussion: Jigsaw puzzling and MG. In Jigsaw puzzling, 3D volumetric data is always split into dozens of cubes that are then shuffled in one of the hundreds of orders. There is a high probability that a cube contains only a small branch of an organ. Hence, it is unjustified to force the network put dozens of cubes in exactly the right order. Actually, some small misaligned cubes do not affect the main anatomy at all. In MG, the network is tasked with recovering every pixel in the medical data even if some patch is meaningless for clinical diagnosis. There are many possible appearances for masked areas in line with the correct anatomical structure rather than only the original ground truth. Due to such rigid self-labelling, the network tends to either find shortcuts or trivial solutions to solve the SSL task or just overfit the

training labels, which is incapable of mining useful information for target tasks. Therefore, we believe it is necessary to develop SSL tasks to focus on salient prior knowledge, such as constructing surrogate labels with some variability but still obeying the pathological prior.

Recently, there is a growing interest in integrating different SSL tasks into a framework to achieve better performance (Dong et al., 2021; Taher et al., 2022), e.g. combining contrastive and generative tasks to learn both global and fine-grained features. We admit that multi-task learning prevents representations from being skewed toward a particular pretext task and pushes the representations to be more robust and high-quality. However, such paradigms render the self-training stage complicated and costly. Besides, the weight of each sub-task is non-trivial to search (Jin et al., 2021). We expect to see more simple yet effective work for medical imaging in the future.

### 8.2. *The objective value of SSL for medical applications*

Compared with natural images, medical images have two characteristics that challenge the performance and training efficiency of deep learning: (1) small data scale caused by expensive data collection and annotation costs. (2) data bias arising from minority disease cases in clinical routine inspection or small lesion areas in the whole imaging region; Most of the existing works have demonstrated the advantages of SSL in mitigating the issue (1), whereas fewer works have systematically assessed the implications of SSL on the issue (2). Based on our extensive experiments, we rethink the value of SSL in both aspects:

- There is now broad consensus that SSL yields better performance in downstream tasks with very limited labelled data (maybe only a few dozen samples), but the returns are diminishing as the downstream labelled training set grows in size (Tajbakhsh et al., 2019; Taleb et al., 2020). In our implementations, we make full use of each medical dataset and find that the improvement from a majority of proxy tasks is marginal in some applications. In each task, the discrepancy between several SSL methods is also small. Thus, the current SSL technique is more meaningful for small-sized datasets. As the community of medical vision expands, medical image datasets of larger size have been or are being created. To achieve remarkable results on moderately-sized annotated medical datasets, it is still a long way to go for SSL.
- Our theoretical model in Section 4 shows that both the class imbalance in labelled data and the potential data imbalance in unlabeled data used for SSL pretraining affect the estimation of the target classifier. Although the modeling in deep networks is much more complex than our assumed theoretical model, we can get a clear intuition of how SSL behaves under data imbalance. Our experiment results confirm that SSL significantly boosts the performance of rare classes but yields marginal impact on frequent classes in both classification and segmentation tasks, thereby improving class-imbalanced learning. This phenomenon seems to reveal the essence of SSL, which is to prevent the network from overfitting to frequent samples. It is natural to ask if we could leverage other commonly used strategies to improve the overfitting issue, including data resampling and data augmentation. For that purpose, we investigate the additive effect of SSL with mean resampling and augmentation policies, respectively. The former results indicate that the performance of SSL can be compounded by mean resampling under extreme data imbalance. However, SSL pretraining is worthless and the simple mean-resampling performs well when the data imbalance is not severe. The latter results suggest that the value of SSL loses when using stronger data augmentation. This enlightens researchers to regard SSL pretraining as a tool to avoid network overfitting to frequent classes. However, it remains a mystery why some SSL methods yiled poorer performance than the baseline when using strong augmentation. This phenomenon is consistent with a previous finding in (Zoph et al., 2020) that supervised pretraining also hurts the downstream performance when using strong augmentation. We believe this is not a coincidence and the interplay between pretraining and data augmentation worth deeper analysis.

### 8.3. Toward better transfer schemes from SSL pretrained models to downstream medical tasks

The success of SSL pretraining depends on not only an effective representation learning via self-supervision signals but also how well the pretrained weights are reused in downstream learning. Looking back, we notice that the transfer process was often neglected in the previous literature. To find better transfer schemes, we discussed two relevant aspects in Section 5.1. First, we explore the role of each module in the pretrained model with a U-shape architecture, including encoder, decoder, the skip connections and BN layers. The results show that the pretrained encoder is exactly what needs to be transferred. On the contrary, the pretrained decoder is dispensable, which contradicts claims from some SSL works that the pretrained decoder is superior to a randomly-initialized decoder (Tao *et al.*, 2020b). Given the lack of experimental verification in these works, our finding is more convincing. Besides, we prove that removing the skip connections in generative SSL leads to better representations in the encoder. As for the BN layers, we recommend to re-collect BN statistics for target data at the test stage since the domain gap between the source data and the target data might degrade performance. Second, we compare different fine-tuning schemes used in previous works. It turns out that full fine-tuning with a small learning rate is the best choice currently.

Despite our recommendations for professionals on better implementations of transfer, there is a large room for future researchers to design better weight reuse schemes. One potentially useful direction is the development of adaptive optimizers that can adjust the learning rate of different parameters according to their behaviours in downstream training, ensuring that expressive pretrained representations are retained and under-learnt representations are updated. Another research direction is to design multi-channel BN layers oriented to different learning stages, following some domain adaptation techniques (Chang *et al.*, 2019; Zhou *et al.*, 2022). Overall, we believe there is an urgent need for research teams to improve current transfer learning paradigms.

## 9. Conclusion

We systematically examine the value of SSL in medical image analysis and present practical guidelines for SSL professionals throughout the entire pre-training and fine-tuning process. On the positive side, we have demonstrated the impressive achievements of SSL in advancing class-imbalanced learning. This is of great clinical value because the diagnosis rate of true positive disease cases is crucial. However, on the negative side, we argue that SSL pretraining is not useful always: (1) the benefits of SSL can be superseded by other frequently-used strategies in some applications, such as data resampling and augmentation. (2) the performance gains from SSL is very limited in middle-size downstream datasets, compared to the insufficient annotated datasets in previous studies. We hope that our in-depth study based on around 250 experiments running over 2000 GPU hours will help to access better capabilities of SSL and shed light on promising research directions for the community to move forward.

## References

Antonelli, M., Reinke, A., Bakas, S., Farahani, K., Kopp-Schneider, A., Landman, B.A., Litjens, G., Menze, B., Ronneberger, O., Summers, R.M., *et al.*, 2022. The medical segmentation decathlon. *Nature Communications* 13, 1–13.

Arjovsky, M., Chintala, S., Bottou, L., 2017. Wasserstein generative adversarial networks, in: International conference on machine learning, PMLR. pp. 214–223.

Armatto III, S.G., McLennan, G., Bidaut, L., McNitt-Gray, M.F., Meyer, C.R., Reeves, A.P., Zhao, B., Aberle, D.R., Henschke, C.I., Hoffman, E.A., *et al.*, 2011. The lung image database consortium (lidc) and image database resource initiative (idri): a completed reference database of lung nodules on ct scans. *Medical physics* 38, 915–931.

Asano, Y.M., Rupprecht, C., Vedaldi, A., 2019. A critical analysis of self-supervision, or what we can learn from a single image. *arXiv preprint arXiv:1904.13132*.

Azizi, S., Mustafa, B., Ryan, F., Beaver, Z., Freyberg, J., Deaton, J., Loh, A., Karthikesalingam, A., Kornblith, S., Chen, T., *et al.*, 2021. Big self-supervised models advance medical image classification, in: Proceedings of the IEEE/CVF International Conference on Computer Vision, pp. 3478–3488.

Bai, W., Chen, C., Tarroni, G., Duan, J., Guitton, F., Petersen, S.E., Guo, Y., Matthews, P.M., Rueckert, D., 2019. Self-supervised learning for cardiac mr image segmentation by anatomical position prediction, in: MICCAI, Springer. pp. 541–549.

Benčević, M., Habijan, M., Galić, I., Pizurica, A., 2022. Self-supervised learning as a means to reduce the need for labeled data in medical image analysis. *arXiv preprint arXiv:2206.00344*.

Bilic, P., Christ, P.F., Vorontsov, E., Chlebus, G., Chen, H., Dou, Q., Fu, C.W., Han, X., Heng, P.A., Hesser, J., *et al.*, 2019. The liver tumor segmentation benchmark (lits). *arXiv preprint arXiv:1901.04056*.

Blendowski, M., Nickisch, H., Heinrich, M.P., 2019. How to learn from unlabeled volume data: Self-supervised 3d context feature learning, in: MICCAI, Springer. pp. 649–657.

Cao, K., Wei, C., Gaidon, A., Arechiga, N., Ma, T., 2019. Learning imbalanced datasets with label-distribution-aware margin loss. Advances in neural information processing systems 32.

Chaitanya, K., Erdil, E., Karani, N., Konukoglu, E., 2020. Contrastive learning of global and local features for medical image segmentation with limited annotations. Advances in Neural Information Processing Systems 33, 12546–12558.

Chang, W.G., You, T., Seo, S., Kwak, S., Han, B., 2019. Domain-specific batch normalization for unsupervised domain adaptation, in: Proceedings of the IEEE/CVF conference on Computer Vision and Pattern Recognition, pp. 7354–7362.

Chen, L., Bentley, P., Mori, K., Misawa, K., Fujiwara, M., Rueckert, D., 2019. Self-supervised learning for medical image analysis using image context restoration. Medical image analysis 58, 101539.

Chen, T., Kornblith, S., Norouzi, M., Hinton, G., 2020a. A simple framework for contrastive learning of visual representations, in: International conference on machine learning, PMLR. pp. 1597–1607.

Chen, X., Fan, H., Girshick, R., He, K., 2020b. Improved baselines with momentum contrastive learning. arXiv preprint arXiv:2003.04297 .

Chen, X., He, K., 2021. Exploring simple siamese representation learning, in: Proceedings of the IEEE/CVF Conference on Computer Vision and Pattern Recognition, pp. 15750–15758.

Chen, X., Wang, X., Zhang, K., Fung, K.M., Thai, T.C., Moore, K., Mannel, R.S., Liu, H., Zheng, B., Qiu, Y., 2022. Recent advances and clinical applications of deep learning in medical image analysis. Medical Image Analysis , 102444.

Chowdhury, A., Rosenthal, J., Waring, J., Umeton, R., 2021. Applying self-supervised learning to medicine: review of the state of the art and medical implementations, in: Informatics, MDPI. p. 59.

Çiçek, Ö., Abdulkadir, A., Lienkamp, S.S., Brox, T., Ronneberger, O., 2016. 3d u-net: learning dense volumetric segmentation from sparse annotation, in: MICCAI, Springer. pp. 424–432.

Doersch, C., Gupta, A., Efros, A.A., 2015. Unsupervised visual representation learning by context prediction, in: Proceedings of the IEEE international conference on computer vision, pp. 1422–1430.

Dong, N., Kampffmeyer, M., Voiculescu, I., 2021. Self-supervised multi-task representation learning for sequential medical images, in: Joint European Conference on Machine Learning and Knowledge Discovery in Databases, Springer. pp. 779–794.

Drozdzal, M., Vorontsov, E., Chartrand, G., Kadoury, S., Pal, C., 2016. The importance of skip connections in biomedical image segmentation, in: Deep learning and data labeling for medical applications. Springer, pp. 179–187.

Ericsson, L., Gouk, H., Hospedales, T.M., 2021. How well do self-supervised models transfer?, in: Proceedings of the IEEE/CVF Conference on Computer Vision and Pattern Recognition, pp. 5414–5423.

Fukunaga, K., 2013. Introduction to statistical pattern recognition. Elsevier.

Goyal, P., Mahajan, D., Gupta, A., Misra, I., 2019. Scaling and benchmarking self-supervised visual representation learning, in: Proceedings of the ieee/cvf International Conference on computer vision, pp. 6391–6400.

Grill, J.B., Strub, F., Altché, F., Tallec, C., Richemond, P., Buchatskaya, E., Doersch, C., Avila Pires, B., Guo, Z., Gheshlaghi Azar, M., et al., 2020. Bootstrap your own latent-a new approach to self-supervised learning. Advances in neural information processing systems 33, 21271–21284.

Haghghi, F., Hosseinzadeh Taher, M.R., Zhou, Z., Gotway, M.B., Liang, J., 2020. Learning semantics-enriched representation via self-discovery, self-classification, and self-restoration, in: MICCAI, Springer. pp. 137–147.

Haghghi, F., Taher, M.R.H., Gotway, M.B., Liang, J., 2022. Dira: Discriminative, restorative, and adversarial learning for self-supervised medical image analysis, in: Proceedings of the IEEE/CVF Conference on Computer Vision and Pattern Recognition, pp. 20824–20834.

Hariharan, B., Arbeláez, P., Girshick, R., Malik, J., 2015. Hypercolumns for object segmentation and fine-grained localization, in: Proceedings of the IEEE conference on computer vision and pattern recognition, pp. 447–456.

He, J., Kortylewski, A., Yang, S., Liu, S., Yang, C., Wang, C., Yuille, A., 2021. Rethinking re-sampling in imbalanced semi-supervised learning. arXiv preprint arXiv:2106.00209 .

He, K., Fan, H., Wu, Y., Xie, S., Girshick, R., 2020. Momentum contrast for unsupervised visual representation learning, in: Proceedings of the IEEE/CVF conference on computer vision and pattern recognition, pp. 9729–9738.

He, K., Zhang, X., Ren, S., Sun, J., 2015. Delving deep into rectifiers: Surpassing human-level performance on imagenet classification, in: Proceedings of the IEEE international conference on computer vision, pp. 1026–1034.

Hosseinzadeh Taher, M.R., Haghghi, F., Feng, R., Gotway, M.B., Liang, J., 2021. A systematic benchmarking analysis of transfer learning for medical image analysis, in: Domain Adaptation and Representation Transfer, and Affordable Healthcare and AI for Resource Diverse Global Health. Springer, pp. 3–13.

Islam, A., Chen, C.F.R., Panda, R., Karlinsky, L., Radke, R., Feris, R., 2021. A broad study on the transferability of visual representations with contrastive learning, in: Proceedings of the IEEE/CVF International Conference on Computer Vision, pp. 8845–8855.

Jin, W., Liu, X., Zhao, X., Ma, Y., Shah, N., Tang, J., 2021. Automated self-supervised learning for graphs. arXiv preprint arXiv:2106.05470 .

Komodakis, N., Gidaris, S., 2018. Unsupervised representation learning by predicting image rotations, in: International Conference on Learning Representations (ICLR). pp. 1–11.

Kornblith, S., Norouzi, M., Lee, H., Hinton, G., 2019. Similarity of neural network representations revisited, in: International Conference on Machine Learning, PMLR. pp. 3519–3529.

Larsson, G., Maire, M., Shakhnarovich, G., 2017. Colorization as a proxy task for visual understanding, in: Proceedings of the IEEE conference on computer vision and pattern recognition, pp. 6874–6883.

Li, Y., Wang, N., Shi, J., Liu, J., Hou, X., 2016. Revisiting batch normalization for practical domain adaptation. arXiv preprint arXiv:1603.04779 .

Li, Z., Zhao, W., Shi, F., Qi, L., Xie, X., Wei, Y., Ding, Z., Gao, Y., Wu, S., Liu, J., et al., 2021. A novel multiple instance learning framework for covid-19 severity assessment via data augmentation and self-supervised learning. Medical Image Analysis 69, 101978.

Liu, X., Zhang, F., Hou, Z., Mian, L., Wang, Z., Zhang, J., Tang, J., 2021. Self-supervised learning: Generative or contrastive. IEEE Transactions on Knowledge and Data Engineering .

Navarro, F., Watanabe, C., Shit, S., Sekuboyina, A., Peek, J.C., Combs, S.E., Menze, B.H., 2021. Evaluating the robustness of self-supervised learning in medical imaging. arXiv preprint arXiv:2105.06986 .

Neyshabur, B., Sedghi, H., Zhang, C., 2020. What is being transferred in transfer learning? Advances in neural information processing systems 33, 512–523.

Nguyen, X.B., Lee, G.S., Kim, S.H., Yang, H.J., 2020. Self-supervised learning based on spatial awareness for medical image analysis. IEEE Access 8, 162973–162981.

Noroozi, M., Favaro, P., 2016. Unsupervised learning of visual representations by solving jigsaw puzzles, in: European conference on computer vision, Springer. pp. 69–84.

Oord, A.v.d., Li, Y., Vinyals, O., 2018. Representation learning with contrastive predictive coding. arXiv preprint arXiv:1807.03748 .

Oquab, M., Bottou, L., Laptev, I., Sivic, J., 2014. Learning and transferring mid-level image representations using convolutional neural networks, in: Proceedings of the IEEE conference on computer vision and pattern recognition, pp. 1717–1724.

Pathak, D., Krahenbuhl, P., Donahue, J., Darrell, T., Efros, A.A., 2016. Context encoders: Feature learning by inpainting, in: Proceedings of the IEEE conference on computer vision and pattern recognition, pp. 2536–2544.

Raghuram, M., Zhang, C., Kleinberg, J., Bengio, S., 2019. Transfusion: Understanding transfer learning for medical imaging. Advances in neural information processing systems 32.

Ronneberger, O., Fischer, P., Brox, T., 2015. U-net: Convolutional networks for biomedical image segmentation, in: MICCAI, Springer. pp. 234–241.

Roth, H.R., Lu, L., Farag, A., Shin, H.C., Liu, J., Turkbey, E.B., Summers, R.M., 2015. Deeporgan: Multi-level deep convolutional networks for automated pancreas segmentation, in: MICCAI, Springer. pp. 556–564.

Saunshi, N., Plevrakis, O., Arora, S., Khodak, M., Khandeparkar, H., 2019. A theoretical analysis of contrastive unsupervised representation learning, in: International Conference on Machine Learning, PMLR. pp. 5628–5637.

Schmidhuber, J., 2015. Deep learning in neural networks: An overview. *Neural Networks* 61, 85–117. URL: <https://www.sciencedirect.com/science/article/pii/S0893608014002135>, doi:<https://doi.org/10.1016/j.neunet.2014.09.003>.

Setio, A.A.A., Traverso, A., De Bel, T., Berens, M.S., Van Den Bogaard, C., Cerello, P., Chen, H., Dou, Q., Fantacci, M.E., Geurts, B., et al., 2017. Validation, comparison, and combination of algorithms for automatic detection of pulmonary nodules in computed tomography images: the luna16 challenge. *Medical image analysis* 42, 1–13.

Shurrab, S., Duwairi, R., 2022. Self-supervised learning methods and applications in medical imaging analysis: A survey. *PeerJ Computer Science* 8, e1045.

Sowrirajan, H., Yang, J., Ng, A.Y., Rajpurkar, P., 2021. Moco pretraining improves representation and transferability of chest x-ray models, in: Medical Imaging with Deep Learning, PMLR. pp. 728–744.

Srinivasan, V., Strothoff, N., Ma, J., Binder, A., Müller, K.R., Samek, W., 2021. On the robustness of pretraining and self-supervision for a deep learning-based analysis of diabetic retinopathy. *arXiv preprint arXiv:2106.13497*.

Sriram, A., Muckley, M., Sinha, K., Shamout, F., Pineau, J., Geras, K.J., Azour, L., Aphinyanaphongs, Y., Yakubova, N., Moore, W., 2021. Covid-19 prognosis via self-supervised representation learning and multi-image prediction. *arXiv preprint arXiv:2101.04909*.

Taher, M.R.H., Haghghi, F., Gotway, M.B., Liang, J., 2022. Caid: Context-aware instance discrimination for self-supervised learning in medical imaging. *arXiv preprint arXiv:2204.07344*.

Tajbakhsh, N., Gotway, M.B., Liang, J., 2015. Computer-aided pulmonary embolism detection using a novel vessel-aligned multi-planar image representation and convolutional neural networks, in: MICCAI, Springer. pp. 62–69.

Tajbakhsh, N., Hu, Y., Cao, J., Yan, X., Xiao, Y., Lu, Y., Liang, J., Terzopoulos, D., Ding, X., 2019. Surrogate supervision for medical image analysis: Effective deep learning from limited quantities of labeled data, in: 2019 IEEE 16th International Symposium on Biomedical Imaging (ISBI 2019), IEEE. pp. 1251–1255.

Taleb, A., Loetsch, W., Danz, N., Severin, J., Gaertner, T., Bergner, B., Lippert, C., 2020. 3d self-supervised methods for medical imaging. *Advances in Neural Information Processing Systems* 33, 18158–18172.

Tao, X., Li, Y., Zhou, W., Ma, K., Zheng, Y., 2020a. Revisiting rubik's cube: self-supervised learning with volume-wise transformation for 3d medical image segmentation, in: MICCAI, Springer. pp. 238–248.

Tao, X., Li, Y., Zhou, W., Ma, K., Zheng, Y., 2020b. Revisiting rubik's cube: self-supervised learning with volume-wise transformation for 3d medical image segmentation, in: MICCAI, Springer. pp. 238–248.

Tong, T., Wolz, R., Wang, Z., Gao, Q., Misawa, K., Fujiwara, M., Mori, K., Hajnal, J.V., Rueckert, D., 2015. Discriminative dictionary learning for abdominal multi-organ segmentation. *Medical image analysis* 23, 92–104.

Vu, Y.N.T., Wang, R., Balachandar, N., Liu, C., Ng, A.Y., Rajpurkar, P., 2021. Medaug: Contrastive learning leveraging patient metadata improves representations for chest x-ray interpretation, in: Machine Learning for Healthcare Conference, PMLR. pp. 755–769.

Wei, C., Xie, L., Ren, X., Xia, Y., Su, C., Liu, J., Tian, Q., Yuille, A.L., 2019. Iterative reorganization with weak spatial constraints: Solving arbitrary jigsaw puzzles for unsupervised representation learning, in: Proceedings of the IEEE/CVF Conference on Computer Vision and Pattern Recognition, pp. 1910–1919.

Wu, Z., Xiong, Y., Yu, S.X., Lin, D., 2018. Unsupervised feature learning via non-parametric instance discrimination, in: Proceedings of the IEEE conference on computer vision and pattern recognition, pp. 3733–3742.

Xie, Y., Zhang, J., Liao, Z., Xia, Y., Shen, C., 2020. Pgl: prior-guided local self-supervised learning for 3d medical image segmentation. *arXiv preprint arXiv:2011.12640*.

Xu, J., 2021. A review of self-supervised learning methods in the field of medical image analysis. *Int. J. Image Graph. Signal Process.(IJIGSP)* 13, 33–46.

Yang, Y., Xu, Z., 2020. Rethinking the value of labels for improving class-imbalanced learning. *Advances in neural information processing systems* 33, 19290–19301.

Zhang, R., Isola, P., Efros, A.A., 2016. Colorful image colorization, in: European conference on computer vision, Springer. pp. 649–666.

Zhang, X., Feng, S., Zhou, Y., Zhang, Y., Wang, Y., 2021. Sar: Scale-aware restoration learning for 3d tumor segmentation, in: MICCAI, Springer. pp. 124–133.

Zhao, N., Wu, Z., Lau, R.W., Lin, S., 2020. What makes instance discrimination good for transfer learning? *arXiv preprint arXiv:2006.06606*.

Zhou, H.Y., Lu, C., Yang, S., Han, X., Yu, Y., 2021a. Preservational learning improves self-supervised medical image models by reconstructing diverse contexts, in: Proceedings of the IEEE/CVF International Conference on Computer Vision, pp. 3499–3509.

Zhou, Z., Qi, L., Yang, X., Ni, D., Shi, Y., 2022. Generalizable cross-modality medical image segmentation via style augmentation and dual normalization, in: Proceedings of the IEEE/CVF Conference on Computer Vision and Pattern Recognition, pp. 20856–20865.

Zhou, Z., Sodha, V., Pang, J., Gotway, M.B., Liang, J., 2021b. Models genesis. *Medical image analysis* 67, 101840.

Zhu, J., Li, Y., Hu, Y., Ma, K., Zhou, S.K., Zheng, Y., 2020. Rubik's cube+: A self-supervised feature learning framework for 3d medical image analysis. *Medical image analysis* 64, 101746.

Zhuang, X., Li, Y., Hu, Y., Ma, K., Yang, Y., Zheng, Y., 2019. Self-supervised feature learning for 3d medical images by playing a rubik's cube, in: MICCAI, Springer. pp. 420–428.

Zoph, B., Ghiasi, G., Lin, T.Y., Cui, Y., Liu, H., Cubuk, E.D., Le, Q., 2020. Rethinking pre-training and self-training. *Advances in neural information processing systems* 33, 3833–3845.